The Role of Convection in Redistributing Formaldehyde to the Upper Troposphere over North America and the North Atlantic during the Summer 2004 INTEX Campaign

Alan Fried[1], Jennifer R. Olson[2], Jim Walega[1], Jim H. Crawford[2], Gao Chen[2], Petter Weibring[1], Dirk Richter[1], Chad Roller[1,3], Frank Tittel[4], Michael Porter[5], Henry Fuelberg[5], Jeremy Halland[5], Timothy H. Bertram[6], Ronald C. Cohen[6], Kenneth Pickering[7], Brian G. Heikes[8], Julie A. Snow[9], Haiwei Shen[8], Daniel W. O'Sullivan[10], Bill H. Brune[11], Xinrong Ren[11], Donald R. Blake[12], Nicola Blake[12], Glen Sachse[2], Glenn S. Diskin[2], James Podolske[13], Stephanie Vay[2], Richard E. Shetter[14], Samuel R. Hall[14], Bruce E. Anderson[2], Lee Thornhill[2], Antony D. Clarke[15], Cameron McNaughton[15], Hanwant B. Singh[13], Melody A. Avery[2], Gregory Huey[16], S. Kim[16], and Dylan B. Millet[17]

In Preparation for Submission to JGR
Version June 12, 2007

---

[1] Earth Observing Laboratory, National Center for Atmospheric Research, Boulder, CO
[2] NASA Langley Research Center, Hampton, VA
[3] Ekips Technologies, Norman, OK
[4] Rice University, Houston, TX
[5] Florida State University, Tallahassee, Fl
[6] University of California, Berkeley, Berkeley, CA
[7] NASA Goddard Space Flight Center, Greenbelt, MD
[8] University of Rhode Island, Narragansett, RI
[9] Slippery Rock University, Slippery Rock, PA
[10] United States Naval Academy, Annapolis, MD
[11] Pennsylvania State University, University Park, PA
[12] University of California, Irvine, CA
[13] NASA Ames Research Center, Moffett Field, CA
[14] Atmospheric Chemistry Div., NCAR, Boulder, CO
[15] University of Hawaii, Manoa, Hawaii
[16] Georgia Institute of Technology, Atlantic, GA
[17] Harvard University, Cambridge, MA

Abstract

Measurements of CH_2O from a tunable diode laser absorption spectrometer (TDLAS) were acquired onboard the NASA DC-8 during the summer 2004 INTEX-NA campaign to test our understanding of convection and production mechanisms in the upper troposphere (UT, 6-12-km) over continental North America and the North Atlantic Ocean. Point-by-point comparisons with box model calculations, when MHP (CH_3OOH) measurements were available for model constraint, resulted in a median CH_2O measurement/model ratio of 0.91 in the UT.

Multiple tracers were used to arrive at a set of UT CH_2O background and perturbed air mass periods, and 46% of the TDLAS measurements fell within the latter category. At least 66% to 73% of these elevated UT observations were caused by enhanced production from CH_2O precursors rather than direct transport of CH_2O from the boundary layer. This distinction is important, since the effects from the former can last for over a week or more compared to one day or less in the case of convective transport of CH_2O itself.

In general, production of CH_2O from CH_4 was found to be the dominant source term, even in perturbed air masses. This was followed by production from MHP, methanol, PAN type compounds, and ketones, in descending order of their contribution. In the presence of elevated NO from lightning and potentially from the stratosphere, there was a definite trend in the CH_2O discrepancy, which for the highest NO mixing ratios produced a median CH_2O measurement/model ratio of 3.9 in the 10-12-km range. Discrepancies in CH_2O and HO_2 in the UT with NO were highly correlated and this provided further information as to the possible mechanism(s) responsible. These discrepancies with NO are consistent with additional production sources of both gases involving CH_3O_2 + NO reactions, most likely caused by unmeasured hydrocarbons.

1. Introduction

The companion paper by Fried et al. [2007] discussed the role and importance of formaldehyde, CH_2O, throughout the troposphere. That paper also provided an overview of CH_2O measurements and modeling approaches employed and their comparisons during the Intercontinental Transport Experiment-North America (INTEX-NA). As described in the overview paper by Singh et al. [2007], the INTEX-NA study was carried out during the summer of 2004 (July 1 to August 15, 2004) over North America and the Atlantic Ocean on the NASA DC-8 airplane. The present study utilizes the results presented by Fried et al. [2007] to further examine the role of convection in transporting CH_2O and its precursors to the upper troposphere (UT, defined here as pressure altitudes extending from 6 to 12-km) during the summer of 2004.

There is a growing body of evidence from a number of recent studies that photolysis of additional HO_x ($OH + HO_2$) precursors, such as CH_2O, H_2O_2, and CH_3OOH (methyl hydroperoxide, MHP), which are thought to be transported from lower altitudes or perhaps emitted from subsonic aircraft, as well as photolysis of acetone, take on greater importance in producing HO_x radicals and ultimately O_3 in the upper troposphere [Wennberg et al. 1998; Jaeglé et al. 1997; Prather and Jacob 1997; Brune et al. 1998; Jaeglé et al. 1998a,b; Jaeglé et al. 2000; Faloona et al. 2000; Muller and Brasseur, 1999; 1998; Cohan et al. 1999; Ravetta et al., 2001; Wang and Prinn, 2000; and Crawford et al., 1999]. These studies revealed the importance of deep tropical convection as well as deep convection from the continental boundary layer on upper tropospheric HO_x levels. As discussed by Jaeglé et al. [1998a] and by Muller and Brasseur [1999], ozone production in the upper troposphere is almost directly proportional to the HO_x mixing ratio; 85% to 95% of the total ozone production arises from the reactions of HO_2 with

NO and CH_3O_2 with NO. Thus, a comprehensive knowledge of upper tropospheric HO_x sources is essential for understanding UT O_3.

Although UT measurements of CH_2O, H_2O_2, and MHP have recently been acquired and examined over the Mediterranean basin during the MINOS study [Kormann et al., 2003; and Lelieveld et al., 2002] and over central Europe and the Mediterranean basin during the UTOPIHAN study in the summer [Colomb et al., 2006; and Stickler et al., 2006], there is a paucity of similar measurements and analyses over North America during summer months. These four studies clearly showed that continental convection of polluted boundary layer sources can significantly affect upper tropospheric HO_x levels. While airborne measurements have been acquired for these same three gases over North America and/or over the North Atlantic Ocean on various platforms [Kleinman et al., 2005; Dasgupta et al., 2005; Fried et al., 2002; Y.-N. Lee et al., 1998; Nunnermacker et al., 2004; Wert et al., 2003; and references therein], these measurements and the subsequent analyses have not focused on UT chemistry and the role of convection; all the measurements were acquired below 7 km and more typically at much lower altitudes below ~ 4 km over urban areas. In fact, with the exception of the Jaeglé et al. [2000] study during the SONEX campaign, to our knowledge, there are no comparable UT data to the European studies prior to the INTEX-NA campaign for CH_2O, H_2O_2, and CH_3OOH focusing on North America and the role of convective transport. Moreover, as the SONEX study primarily focused on the North Atlantic during the fall, there is only partial coverage over the continental United States and no coverage during the summer months when photochemical activity is high and deep convection from severe thunderstorm activity over continental North America can be significant.

This study is the last in a series of four papers, based upon observations and model results during the INTEX-NA study examining UT convection of CH_2O. The first paper by Millet et al. [2006], discussed CH_2O distributions over North America and implications for satellite retrievals. The second paper by Snow et al. [2006] showed the importance of convection in transporting the aforementioned gases to the UT and compared and contrasted these results with two other airborne campaigns. The third paper by Fried et al. [2007] discussed two airborne instruments employed during the INTEX-NA study for measuring CH_2O onboard the NASA DC-8 aircraft: a tunable diode laser absorption spectrometer (TDLAS) from the National Center for Atmospheric Research (NCAR), and an automated coil enzyme (CENZ) fluorometric method from the University of Rhode Island. That paper also presented an overview of the comparison between the two instruments, a description of the NASA Langley box model and the GEOS-Chem 3D global transport model [Millet et al., 2006], and an overview of the box model-TDLAS comparisons. The present study utilizes the TDLAS and model results of the third paper by Fried et al. [2007] to further: 1) establish sets of conditions by which to distinguish "background" UT CH_2O levels from those perturbed by convection and other causes; 2) quantify the CH_2O precursor budgets for both air mass types; 3) quantify the fraction of time that the UT CH_2O measurements over North America and the North Atlantic are perturbed during the summer of 2004; 4) provide estimates for the fraction of time that such perturbed CH_2O levels are caused by direct convection of boundary layer CH_2O and/or convection of CH_2O precursors; 5) assess the extent to which box models successfully capture such elevated events in the UT; 6) provide a contrast with UT CH_2O measurements acquired over more remote regions of the Pacific Ocean during the 2001 TRACE-P study; and 7) further examine CH_2O and HO_2 relationships.

2. Modeled Temporal Dependence for Different Injection Scenarios in the UT

Understanding the cause of elevated CH_2O in the UT (4^{th} goal above) is more than of academic interest, as can be seen by the model runs of Fig. 1 and 2. The Langley model was run forward in a time-dependent mode after being initialized with median conditions observed from 8.5 to 9.5-km during INTEX-NA. The figures show resulting time-dependent CH_2O mixing ratios calculated from this "base" box model run (black curve) and for additional model runs assuming various injection scenarios of NO_2, CH_2O and its precursors. The blue curves in Fig. 1 and 2 show results for direct injection of median observed boundary layer CH_2O (2065-pptv). The dashed red curves show the results for injection of a suite of CH_2O precursors (CH_4, MHP, CH_3OH, Acetone, and PAN) also based on median boundary layer mixing ratios, while the solid red curves show results for simultaneous injection of both CH_2O and its precursors. The lower panel in each figure shows the results normalized to the base model run. Figure 1 shows simulations that assume an initial NO_x mixing ratio of 345-pptv (obtained from median observed NO of 250-pptv and a steady-state calculation of NO_2). Figure 2 shows results for the identical injection scenarios described in Fig. 1, but with an additional initial NO_x injection source from lightning assumed here to equal 1-ppbv. In all cases, the model allows for photochemical decay of NO_x and the CH_2O precursor species. The companion paper by Fried et al. [2007] discusses the importance of nitric oxide (NO) from sources such as lightning in accelerating the production of CH_2O, particularly in the UT. This acceleration in CH_2O production can be seen by comparing the precursor-only curves (dashed red lines) in Fig. 1 and Fig. 2 to the base case. One day after initialization, the CH_2O is photochemically enhanced by 60% for the median NO_x scenario and by 90% for the enhanced NO_x scenario. Such enhanced NO accelerates the reaction

of methylperoxy radicals (CH_3O_2), and more generally RO_2 radicals, in ultimately forming CH_2O and HO_2 in the process (Fig. 3).

As can be seen, the base case yields an initial CH_2O mixing ratio of 195-pptv in both figures and this rapidly decays with each diurnal cycle to mixing ratios around 75-pptv in 1 week. The direct injection of boundary layer CH_2O decays to the base case in approximately 1 day after the initial injection for both NO_x scenarios, after which it decays identically with the base case. By contrast, injection of CH_2O precursors, either with CH_2O or precursors alone yields elevated CH_2O for up to one week in all cases. The injection of CH_2O with precursors closely approaches injection of CH_2O precursors alone after approximately 1 day in both NO_x scenarios. The effects of the additional NO_x aren't realized until ~ 1 day downstream of the convective event (compare the ratio to the base case in Fig. 1 relative to Fig. 2), where upon the elevated NO_x curve starts to diverge from the background NO_x case. After 1 week the elevation relative to the base case is ~ 20% for the median NO_x simulations and 40% for the elevated NO_x simulations. Thus, understanding the exact mechanism responsible for elevated CH_2O in the UT is important for understanding its integrated influence and the extent of influence downwind of convection.

The base case plots in both NO_x scenarios also indicate that background CH_2O in the UT over North America and the Atlantic Ocean should reside in the range between 75-pptv and 195-pptv range for air masses up to one week old. Comparisons of these expectations with measurements will be presented in a later section.

3. Measurement Box Model Comparisons for CH_2O in the UT

3.1 Comparisons during Clear versus Non-Clear Conditions

The companion paper by Fried et al. [2007] discussed the CH_2O observations and model results in clear versus non-clear conditions throughout the troposphere and highlighted the

influence of convection in elevating both the observations and model results during non-clear conditions. The delineation between clear and non-clear conditions was determined utilizing measurements of aerosol volume density for particles in 10-20 μm size range in conjunction with the DC-8 videotapes. Most of the non-clear sampling occurred in haze and under intermediate conditions. Only 15% of the non-clear encounters in the UT involved sampling where there was at least 50% cloud coverage. Unfortunately, there were many instances during INTEX-NA where convection affected UT CH_2O mixing ratios but the appearance of clouds, one of the telltale signatures of such events, was no longer present by the time of DC-8 sampling. Fortunately, Fuelberg et al. [2006] developed a methodology based upon a comparison of meteorological trajectory analysis with both Global Forecast System (GFS) modeled fields and data from the National Lightning Detection Network. They produced estimates of when the sampled air mass had previously experienced deep convection or experienced lightning originating within 1.5 degree latitude/longitude grid boxes. Although this procedure does not consider small scale processes such as turbulence that are not handled adequately by the GFS model, it does capture pollution events vertically lofted by processes that are resolvable by the GFS model. In the UT, 78% of the cloud encounters from aerosol volume density measurements, when time coincident TDLAS measurements and box models were available and where measurements of MHP were available for model input, had experienced convective influence according to the Fuelberg et al. analysis. The companion paper by Fried et al. [2007] discussed the importance of MHP measurements in constraining box model calculations, particularly during fresh convection in the UT where model calculations of MHP do not accurately capture the observations. In the present study, except where noted, all UT CH_2O measurement-model comparisons will only consider time periods where MHP data are available for model input. This includes MHP measurements

at their limits of detection (LODs) where convective influence on MHP is not an issue. The remainder of this paper will rely heavily on the Fuelberg et al. [2006] meteorological methodology as an indicator of convection.

Table 1a relates clear and non-clear conditions to the results from the Fuelberg et al. [2006] analysis. This table provides the median values for selected parameters broken out for 3 altitude bins in the UT (6 to 8-km, 8 to 10-km, and 10 – 12-km) only when CH_2O measurement-model comparisons are available and when MHP data are available for model input. We show in this table the median values in time steps of 1 hour before the air sampled by the DC-8 first encountered convection and/or lightning by the Fuelberg et al. meteorological analysis [2006]. We also show in this table the median mixing ratios for the 3 most important constituents (to be discussed) in the production of CH_2O as well as CO mixing ratios as an inert tracer. In no case did emissions from fires play a role in the comparisons here, as indicated by fire tracers HCN and CH_3CN, nor was convection from the boundary or residual layer (maximum height of a few km) important here.

As can be seen in Table 1a, median methane and CO mixing ratios are only slightly elevated for non-clear compared to clear conditions for all three altitude bins. The slightly elevated CO in the 10 – 12-km range indicates the presence of mid-troposphere pollution. By contrast, the median mixing ratios for MHP and methanol (the 2nd and 3rd largest CH_2O precursors in the UT, as will be discussed) become significantly elevated in the non-clear 10-12-km range compared to clear conditions; MHP is enhanced by a factor of 1.9 for these conditions while methanol is enhanced by a factor of 3.8. Just as striking are the median time comparisons since convection and lightning for the 10-12-km range; the median time before convective encounter changes from 12 hours to 4 hours between clear and non-clear conditions and the corresponding lightning

encounter time change from 12 to 1 hour. In addition, both CH_2O observations and box model CH_2O mixing ratios increase by more than a factor of two during non-clear conditions in the 10 – 12-km bin compared to clear conditions. Nevertheless, as shown in Table 1b, the median point-by-point measurement/model ratios are in good agreement for both clear and non-clear conditions for this altitude bin, indicating that the box model in these cases faithfully captures the observations during convective perturbations in the UT.

Table 1b also tabulates the median NO_x values, based upon measurements of NO_2 [Bertram et al., 2007] and photostationary state calculations of NO for the 3 different altitude bins. As discussed by Ren et al. [2007], although direct measurements of NO were in general agreement with the NO_2-derived values, the latter provided more precise values since the direct measurements of NO only had a detection limit of 50-pptv for 1-minute integration times. All further discussions of NO throughout the rest of this paper refer to calculated values using this procedure. As can be seen in Table 1b the NO_x is not significantly different between clear and non-clear conditions for all 3 altitude bins but the absolute value increases by over a factor of 4 between the lowest and highest bins due to lightning and transport from the stratosphere.

While the clear versus non-clear distinctions just discussed provides a useful contrast regarding CH_2O precursor mixing ratios and the resultant measurement/model relationships, in the present study this analysis masks one important aspect: namely, the role of NO in enhancing the production of CH_2O in the UT, and thus in accentuating discrepancies potentially caused by unmeasured species. As discussed previously, effects of convection were still operative in many cases even though the air at the time of sampling was categorized as clear. In fact, contrary to our expectations, the largest enhancements in NO were observed in the 10-12-km altitude range during clear conditions; the number of significantly elevated NO encounters (NO > 1000-pptv)

was a factor of 8 higher here compared to non-clear conditions while the maximum NO values were a factor of 6 higher during clear versus non-clear conditions. The role of NO and how its affects CH_2O measurement-model relationships will be discussed in Section 6.

3.2 UT Measurement/Model Ratios

In Fig 4 we plot the ratios for TDLAS to box model results as a function of pressure altitude for all locations combined with the data parsed into comparisons falling within the combined random measurement-model uncertainties (open points) and those outside this range (filled points). The companion paper by Fried et al. [2007] discusses these uncertainty estimates. All comparisons are shown in the left panel with the exception of 1 point at 11-km (Ratio = 20.8) to maintain resolution. Of the 1642 comparison points, 56% of the data fall within the combined random uncertainties with 20% and 24% showing positive and negative outliers, respectively. When systematic uncertainty estimates are considered, which encompasses uncertainties in the rate constants employed in the box model calculations, 62% of the UT comparisons fall within the combined systematic limits.

The panel on the right side of Fig. 4 further restricts the comparisons to points (N = 1188) in the UT where measurements of MHP are available and used in the box model (including points at the MHP LOD). Although some of the large outliers in the full comparison are removed with this additional parsing, surprisingly this does not improve the overall percentage of comparison points falling within the combined random uncertainty estimates: 56% of the data fall within this limit with 18% and 26% showing positive and negative outliers, respectively. This additional constraint, furthermore, only marginally changed the spread in the measurement/model ratios, and this is shown in Table 2.

In Fig. 5 we show the 6 – 12-km altitude-dependent TDLAS box model outlier ratios only. These are color coded and sized by the time since convection and time since first lightning encounter within a 1.5 deg box as determined from the meteorological analysis by Fuelberg et al. [2006]. Again, the ratios are restricted to points where MHP measurements are available and used in the box model. In many cases the largest outliers are associated with comparison points that have experienced convection and/or lightning within the past 2 hours. It is entirely possible that these points reflect direct convection of boundary layer CH_2O and/or convection of CH_2O precursors; as Fig. 1 shows these two effects become indistinguishable after ~ 1 day following the perturbation. However, there are also exceptions to the above observations in Fig. 5; for example, one can readily spot a number of outlier points between 10 and 12-km with high measurement/model ratios but no convective and/or lightning influence (filled gray triangles) as well as high ratios with convective and/or lightning influence longer than 5 hours at other altitudes. Clearly other factors must be operative here as well as for many of the smaller outlier ratios. In fact only 32% of the UT outliers are influenced by convection and/or lightning within the past 6 hours, 2.6 to 5 CH_2O e-folding lifetimes from Table 1. Moreover, 58% of the UT non-outliers experienced convection and/or lightning within the past 6 hours. For the outlier cases, the median values for the convective and lightning encounters in the UT are 9 and 10 hours, respectively. This compares to median values of 8 and 11 for all UT measurement-model comparisons where MHP is used as a model constraint. Thus, with the exception of the largest outliers associated with very recent perturbations from convection and/or lightning, UT air masses impacted by these perturbations generally are not well correlated with the CH_2O measurement-model agreement. It is entirely possible that some of the convected air, indicated by the meteorological analysis, was transported from mid-altitudes, where in all likelihood there

is minimal elevation in CH_2O and/or its precursors. It is also possible that fresh convection in many cases may be transported with air that is well-aged since time of emission, and depending upon the particular CH_2O source(s) that are present, the box model may or may not faithfully capture such observations. Lastly, as no trajectory model is perfect, one can encounter errors in the exact placement of convection, and these increase with time since convection. The three case studies in Section 7 will further elucidate various measurement-model behaviors for different convection scenarios.

4. Background and Perturbed CH_2O Levels in the UT

In this section we derive estimates for the percentage of time UT perturbations of CH_2O are associated with transport of CH_2O precursors. As was pointed out previously, direct transport of CH_2O will in many cases be associated with transport of CH_2O precursors to the UT as well. These two effects become indistinguishable after ~ 1 day following the convection, and as shown in Fig. 1, behave like convection of CH_2O precursors only, which can yield significant perturbations out to 1 week or more. We thus provide estimates in this section for the percentage of time UT CH_2O perturbations are associated with precursors, without distinguishing if direct transport of CH_2O is simultaneously present.

To accomplish this we first determine a set of background conditions for the UT over North America and the Atlantic Ocean during summer months. This is based upon a variety of tracers for CH_2O, anthropogenic pollution, and biomass burning influences, and these are listed in Tables 3a and 3b. Table 3a lists 15 primary species and their UT mixing ratios at the 25 percentile level for all measurements during INTEX-NA (not restricted to geographic location or time periods when TDLAS measurement and/or box model results are present). Table 3b lists additional species used in helping with this determination. In both tables measurements at their

LODs were included in this analysis by replacing the LOD flags with LOD mixing ratios. The UTOPIHAN II study by Stickler et al. [2006] over central-western Europe and the northwest Mediterranean mid to upper tropospheric region used many of the same tracers with similar magnitudes as Table 3a and 3b to help in defining background conditions for a select set of measurements. With the exception of CO_2 and O_3, air masses with mixing ratios for these various species above their respective 25% threshold levels were eliminated from the clean background category. Despite the fact that this 25% cutoff limit is somewhat arbitrary, it is important to note that many of the background tracer levels were in fact below their 10 percentile UT levels.

Since not all tracers were always present and/or revealed a consistent picture (i.e., some tracers were elevated while others were below the 25% threshold level), judgment calls were frequently made and the 25% cutoff limits were used as a guide. However, in this vetting we generally sided with being too strict (i.e, removed too much data) in order to obtain the best determination for background UT conditions. The 15 primary species in Table 3a were given the most weight followed by the additional 11 species in Table 3b. In a number of cases O_3 was elevated while CO was not, indicating stratospheric air, which was still considered for the background category. As discussed previously, a depressed UT CO_2 mixing ratio is one indicator of boundary layer influence due to photosynthetic activity, and in this case CO_2 mixing ratios less than the lowest 25% levels were eliminated. This vetting process resulted in 105 "clean background" UT time periods where convection and lightning did not perturb the UT CH_2O data.

Next we further examined these 105 UT air masses using FLEXPART trajectories employing the retroplume tool from Stohl et al. [1998] as well as the "age since convection" tool based upon NO_x/HNO_3 ratios developed by Bertram et al. [2007]. Any air mass whose trajectory originated from the boundary layer within the past 5 days or experienced convection (using the Bertram

ratios) over the past 3 days was further eliminated. This resulted in a more restrictive set of 77 UT aged "clean background" time periods during INTEX-NA, which we hereafter refer to as "background" time periods.

Figure 6 displays the resulting CH_2O TDLAS measurements (N = 68), box model results (N = 62), CENZ measurements (N = 18), and GEOS-Chem 3-D model results (N = 77) for these UT time periods. As indicated by the inset in Fig. 6, the majority of the UT background air masses were sampled over central to eastern North America, but there were also points off the United States coast and out over the more remote Atlantic Ocean. The shaded region (-56 to 165 pptv) highlighted in Fig. 6 captures most of the measurements and model results for the 6 – 12 km UT range. Although the precise upper limit is somewhat subjective, the present upper limit of 165-pptv captures 99% of the composite measurements and box model results and excludes some of the clear outlier points, which are primarily from the GEOS-Chem model; 13 of the GEOS-Chem model results lie outside the 165-pptv limit. These 77 background data points were further checked using the meteorological analysis of Fuelberg et al. [2006], which further indicated that none of the 77 air mass time periods was influenced by the boundary or residual layers over the past 24 hours. Although 16 of the 77 time periods experienced some convection from this analysis, back trajectories indicated the air in all cases remained above 6-km within the past 24-hours, and eliminating these points only negligibly affected the determined upper limit (168-pptv versus 165-pptv).

The background CH_2O levels of Fig. 6 (-56 to 165-pptv) are consistent with the base case levels of Figs. 1 and 2; in the absence of perturbations caused by convection and other causes, the time dependent model calculations in these figures are close to the background levels of Fig. 6 at the start of the calculation (195-pptv) and fall within the background range of Fig. 6 after

only ~ 6-hours of decay. Based upon the median measurements and box model values of Fig. 6 (range: 29 to 77-pptv) the time dependent calculations suggest a median air mass age of at least 6.8-days for these UT background air masses.

Figure 7 displays all the TDLAS, and CENZ measurements and box model results acquired in the 6 – 12 km UT range during INTEX-NA for all data in the database not parsed by location, nor restricted for time coincidence and/or the availability of MHP for model input. The (-56 to 165-pptv) background limits defined above are superimposed on these plots to emphasize in all three cases: 1) the large number of points falling within the background range (to be discussed); and 2) the large number of perturbed UT observations outside this range, the percentages for which are indicated in the plots for all three cases. Out of a total of 2906 TDLAS measurements of CH_2O in the UT, 46% lie outside the positive upper background limit. This compares to 42% and 38%, respectively, for the box model and CENZ measurements. The GEOS-Chem model results, which are not shown, indicate that 40% of the results fall outside the background limits. Taken together, all 4 data sets indicate that ~ 40% of the UT observations and/or model results for CH_2O reveal perturbations relative to background conditions (i.e., exceed the 165-pptv upper bound for background conditions). These perturbations include: convectively influenced air both with and without biomass burning influence as well as perturbations from other causes. Even though Fig. 7 is not restricted for time coincidence, many of the perturbations appear to be common to all three data sets; the perturbations around 10.7-km, 10-km, 9.3-km, and 7-km are examples of this.

Figure 8 plots the altitude dependence of the UT TDLAS CH_2O measurements, which are time coincident with the box model calculations that employ MHP as input (N = 1188). Similar to Fig. 7, Fig. 8 shows the background range superimposed for reference. The points are color

coded and sized by the box model CH_2O production rates, the maximum value for which during the strict 77 background selected air parcels is $3.51x10^5$ molecules cm^{-3} sec^{-1} (designated by the vertical line in the color scale). Many of the elevated perturbed TDLAS observations also show elevated box model production rates that are greater than the maximum value observed during background conditions. Conversely, nearly all the data within the background limits show low box model production rates.

In general, we can state the following: although the TDLAS measurements are as high as 20.8 times the box model result, most of the UT measurements are in good agreement with the box model; the median UT measurement/model ratio is 0.91 for the 1188 comparisons where measured MHP was employed in the calculations. Even in many of the cases where there are large measurement-model discrepancies, the box model production rates for CH_2O are higher than the maximum value of $3.51x10^5$ molecules cm^{-3} sec^{-1} determined for background conditions. Thus, the box model production rates can be used as one means to estimate a lower limit for the percentage of time that elevated UT CH_2O observations are associated with enhanced production from CH_2O precursors. Direct convection of CH_2O alone from lower altitudes would affect the TDLAS measurements but not the box model production rates.

Averaged over the entire UT 6 – 12-km range, 66% of the perturbed elevated TDLAS measurements (TDLAS > 165-pptv, where MHP is used to constrain the box model) have elevated box model production rates associated with CH_2O precursor transport. Here we define elevated box model production rates as those higher than the maximum background CH_2O production rates for the three UT altitude bins expressed in pptv sec^{-1} (6-8 km: 0.029 pptv sec^{-1}; 8-10-km: 0.027 pptv sec^{-1}; 10-12-km: 0.027 pptv sec^{-1}). Expressing the production rates this way is necessary to account for the changing number density with altitude. Parsing the UT range into

the three altitude bins, we find that 66%, 72%, and 53% of the elevated TDLAS measurements are associated with enhanced model production rates for respectively the 6-8 km, 8 – 10 km, and 10 – 12 km, altitude ranges.

In a second determination, we estimate the percentage of time UT perturbations of CH_2O are caused by CH_2O precursors employing the convective products from Fuelberg et al. [2006]. In this approach, we deduce the fraction of the perturbed UT TDLAS measurements (measurements > 165-pptv) that show convective influence from the Fuelberg et al. analysis greater than a certain characteristic time since convection. This approach relies on the fact that after this characteristic time, direct convection of CH_2O from lower altitudes quickly decays to background levels due to the short CH_2O lifetime, as is shown by Fig. 1. We determined this characteristic time using Expressions (3) and (4) below. Expression (3), which is derived by Bertram et al. [2007], relates the UT mean mixing ratio for a species in fresh convective outflow at time zero ($[CH_2O]_{UT\ (t=0)}$) to the fraction (f) of the boundary layer air present in the fresh convection and the UT mixing ratio in the background air ($[CH_2O]_{UT}$) in accordance with:

$$[CH_2O]_{UT\ (t=0)} = f[CH_2O]_{BL} + (1-f)[CH_2O]_{UT} \quad (3)$$

Using a value of f = 0.20 ± 0.1, determined by Bertram et al. [2007], a median TDLAS measured value of 29-pptv for background air in Fig. 6, a median TDLAS boundary value of 2065-pptv, we determine a value of 436 ± 204-pptv for $[CH_2O]_{UT\ (t=0)}$. During daylight hours, the time (t) for this fresh direct boundary layer CH_2O convection to decay to the background threshold value of 165-pptv ($[CH_2O]_{Bkg\ Threshold}$) is determined by:

$$[CH_2O]_{Bkg\ Threshold} = (436 \pm 204)\ \exp\text{-}(t/\tau) \quad (4)$$

Using a median mid-day UT CH_2O lifetime (τ) of 1.5 hours we determine a characteristic time t of 1.5-hours (range 0.5 to 2-hours) for the time it should take for the average fresh convective

outflow in the UT to decay below the background threshold level. Perturbed UT CH_2O observations whose time since convection are greater than 1.5-hours can be ascribed to in situ production of CH_2O from its precursors. Of the TDLAS CH_2O observations (where there are measurements of MHP to constrain the box model, and where there is convective influence) in perturbed UT air, 73% fall in this category. This value is in reasonable agreement with the 66% value determined by elevated model production rates. For the remaining 27% to 34% of the time our perturbed UT observations can be ascribed to direct CH_2O convection and/or convection of CH_2O precursors. At present there is no way to pull these two effects apart, and thus CH_2O precursors may be playing an even larger role in the UT. The one drawback of the present analysis is that it assumes a CH_2O lifetime of 1.5-hours, which is characteristic of mid-day. Convection at time periods later in the day or during the previous night would yield longer characteristic times with a consequent lower value for the precursor percentage. Fortunately the local sun time when most of the convection during INTEX-NA was sampled (for time coincident measurement and box model periods) was between 12 noon and 1 PM, and thus the error from this cause is small in most cases. This procedure is also not that sensitive to the precise background cutoff limit. If the true background cutoff limit for CH_2O is 100-pptv instead of 165-pptv, this would only change the precursor percentage determination from 73% to 74%. A 200-pptv cutoff limit changes this 72%. We also used the above procedure to determine the perturbation percentage due to precursors broken out for the three different altitude bins in the UT and this yields the following: 72% for 6-8-km, 72% for 8-10-km, and 80% for 10-12-km.

As discussed in the companion paper by Fried et al. [2007], the meteorological analysis from Fuelberg et al. [2006] indicated that 2004 was a record breaking year for wildfire activity in northwest Canada and Alaska and these plumes were sampled by the DC-8 on numerous flights.

Although this can perturb the chemistry of the UT, we are more interested in the present study in characterizing the more ubiquitous UT perturbations from convection. To accomplish this we use PAN, HCN, CH_3CN, and CO as tracers of fire plumes. Specifically, we have identified cases where these 4 tracers exceeded their UT 99th percentile values of: PAN (951-pptv), HCN (755-pptv), CH_3CN (306-pptv), and CO (219-ppbv). For example, during the July 18 Alaskan fire plume intercept shown in Fig 5b of the companion paper by Fried et al. [2007] at 7-km, these 4 fire plume tracers attained values as high as 1574-pptv for PAN, 2740-pptv for HCN, 1318-pptv for CH_3CN, and 400-ppbv for CO. After removing the few UT points that are clearly affected by fire plumes, the above percentages for transport of CH_2O precursors are negligibly changed by less than 1% for all 3 altitude bins.

5. UT Budgets for Production of CH_2O during Background & Perturbed Periods

An examination of Fig. 7 and 8 immediately reveals that there are a significantly larger number of measurements and box model results that fall within the UT background limits than indicated by the strict 77 time periods discussed above. For example, as shown in Fig. 6, there are 69 TDLAS measurements that satisfy the strict background limit, yet there are a total of 1579 UT TDLAS measurements with CH_2O levels less than the 165-pptv background limit. In the case of the box model and CENZ measurements, there are 62 and 18 time periods, respectively, satisfying the strict background limit, and this compares to 1320 and 717 points for levels less than the 165-pptv limit. In some cases there are not enough tracers for the formal background label to be applied, while in other cases elevated longer-lived tracers are still present but the air mass is sufficiently well-aged that the ambient CH_2O levels decay down to background levels. Rather than restrict our discussion of UT CH_2O budgets to a small number of air masses obeying the strict background limit (there are only 55 time coincident TDLAS and box model results in

this category), where for example the negative TDLAS measurements may exert an undue influence, we employ here a less rigorous surrogate definition for background and perturbed UT cases based upon modeled CH_2O levels. Air masses where the time coincident CH_2O mixing ratios for the box model results (where MHP is used to constrain the model) are equal to or below 165-pptv will henceforth be classified as background (49% of UT time coincident comparisons), regardless of the tracer levels in Tables in 3, and those where the model exceeds this limit are classified as perturbed (51% of UT time coincident comparisons).

Table 4a compiles the mean, standard deviation, median, and number of time coincident TDLAS and box model results for the 6-8-km, 8-10-km, and 10-12-km pressure altitude bins in the UT for the background and perturbed air masses as defined above. In the 10-12-km range for the perturbed case, there were 27 additional time periods where the NO mixing ratios were all larger than 1000-pptv, the box model values were below the 165-pptv cutoff limit, and in most cases the measured CH_2O values were all above this limit. These 27 points were added to the original 42 comparison points, and accounts for the fact that the box model and observations diverge under high NO_x conditions. This will be further discussed in Section 6. Elevated NO_x, which is caused by convection, lightning, and potentially stratospheric intrusions, enhances CH_2O production (see Fig. 3). Only perturbed time periods in the 10-12 altitude bin were affected by this. Without this correction, the median point-by-point measurement/model ratio shown in Table 4b would be erroneously lowered from 1.3 to 1.2. Considering only NO mixing ratios greater than 1000-pptv in the 10-12-km perturbed bin, the median measurement/model ratio increases to 1.8.

Our background/perturbed segregation approach has ambiguities in cases: 1) where the measurements are perturbed (TDLAS > 165-pptv) relative to background box model results

(28% of the UT time coincident comparisons), and 2) alternatively where the measurements fall in the background range while the model results are perturbed (35% of the comparisons). The first, as discussed above, tends to deemphasize the magnitude of the convective perturbations. Data in the second category, which includes data affected by uptake, would do the opposite. Despite these caveats this segregation approach provides a useful way to contrast CH_2O production terms from the various hydrocarbon precursors between perturbed and background air masses.

As shown in Table 4, the median TDLAS and box model mixing ratios are comparable for all cases with the exception of the perturbed 10-12-km bin. With the exception of this bin, the differences (TDLAS-Box Model) of the medians in Table 4a are all small and range between -18-pptv to -31-pptv. Table 4b tabulates statistics directly for the point-by-point (TDLAS-Box Model) differences, and again the median values for these 5 bins are all small and slightly negative: here the differences range between -10 to -31-pptv and the median TDLAS/Box Model ratios range between 0.72 and 0.96. For the perturbed 10 – 12-km altitude case, the median point-by-point difference is slightly elevated (64-pptv) relative to the other cases (ratio = 1.3). Here the median NO_x levels are significantly elevated (1391-pptv) relative to the other cases. This will be further discussed in Section 6.

During the UTOPIHAN II campaign, Stickler et al. [2006] measured UT CH_2O background mixing ratios in the range between ~ 25-pptv and 150-pptv at ~ 8-km. During a second flight at ~ 8-km, identified by these authors as convectively influenced, the CH_2O mixing ratios attained values as high as ~ 1000-pptv and averaged around 300-pptv. Both are similar in magnitude to those of the present study. Kormann et al. [2003] during the summer of 2001 MINOS campaign over the eastern Mediterranean also identified time periods where UT CH_2O mixing ratios were

reflective of the air mass origin. One flight in particular was identified as originating from the western Atlantic Ocean and produced mean CH_2O mixing ratios ranging between 114 to 281-pptv for the 6 to 12-km altitude range. Although somewhat higher than the overall INTEX-NA background levels observed here, the lower limit falls within the range of values observed in this study. During a second flight, where the air originated from Indian monsoon outflow, the mean UT CH_2O levels ranged between 703 to 1276-pptv. Although this is considerably higher than the overall INTEX-NA means shown in Table 4a for the perturbed measurements, such measurements fall within the -88 to 1549-pptv range (not shown) observed in this study for perturbed conditions in the UT.

Figure 9a plots the median UT CH_2O production rates (in pptv sec^{-1}) for time coincident TDLAS and box model results where MHP measurements are used in the model constraint. The production rates are from the box model runs for the major production terms only. Contributions from alkenes, alkanes, isoprene, ethene, aromatics, acetic acid, and acetaldehyde are calculated but are too low to be included in Fig. 9a. This plot shows the data parsed into background and perturbed air masses, as defined above, for each of the three altitude bins in the UT. The production rates are for the parent species shown. For example, the reaction between CH_3O_2 and NO is involved in the production of CH_2O from most of the species shown, and the model was run by ascribing the contributions for this reaction to each of the CH_2O precursors in Fig. 9a. The PAN term includes PAN and reactions for RCO_3 type compounds. The ketones term includes acetone as well as other ketones. The numbers above each component represent the production percentage for that air mass type in the given altitude bin. The percentages for the major species shown comprise 83% to 92% of the total CH_2O production.

As can be seen in Fig. 9a, in all cases CH_2O production from CH_4 is the major term, even in perturbed air masses on average. In general this is followed by production from MHP (CH_3OOH), MeOH (methanol), PANS, and ketones. The total CH_2O production rate expressed in mixing ratio per unit time as a function of altitude has a number of competing terms. On one hand the production rate should drop off with altitude due to the strong temperature dependence for the reaction between CH_4 and OH; there is a factor of 2 drop in this reaction rate in the 10-12-km bin compared to the 6-8-km bin. This is countered by a factor of ~ 1.5 to 2 increase in OH number density and ~ an order of magnitude increase in NO_x between these two altitudes (see tables 4b and 4c). As can be seen in Fig. 9a, in the background cases these effects offset and the total CH_2O production rates are essentially constant with altitude. For the perturbed cases there is a slight change with altitude (factor of 12% for the two altitudes in question) due to enhanced: NO_x, OH, and methanol (see Fig. 9b) with altitude. The production rates are over a factor of 2 higher in perturbed cases relative to background at all altitudes. Figure 9b shows the corresponding mixing ratios for CH_2O along with those involved in the 3 major production terms (CH_4, MHP, and Methanol) plus NO_x in the same format as Fig. 9a. The corresponding mixing ratios for OH, which are not shown in Fig. 9b to avoid clutter, are given in Table 4c.

The enhanced NO_x with altitude in part reflects the fact that both perturbed and background air masses in the UT are in many cases influenced by lightning. Based upon the meteorological analysis from Fuelberg et al. [2006] employing 1.5 x 1.5 degree grid boxes, we find that for the UT data being considered (N = 1188 between 6 and 12-km where there are measurements and modeled CH_2O using measured MHP as a constraint) 90% of the perturbed air masses in the 10-12-km range have been influenced by lightning within the past 24-hours (median influence within past 2 hours before sampling) and this compares to 50% for background conditions

(median influence within past 13 hours before sampling). Furthermore, such influence decreases with decreasing altitude. For the 6-8-km range, 53% and 27% of the perturbed and background air masses, respectively, have been influenced by lightning within the past 24-hours.

The above observations with respect to OH and NO_x also explain the fact that median ratios between perturbed and background production rates for methane are a factor of ~ 2 for all UT altitudes whereas the methane mixing ratios are only negligibly changed between these two air mass types.

It is instructive to compare the CH_2O production budgets of Fig. 9a to those determined by Stickler et al. [2006] in the UT over central-western Europe and the northwestern Mediterranean region. During background and convectively influenced time periods between 6 and 7-km, Stickler et al. determined production percentages from CH_4 ranging between 26% to 40% and 29% to 44%, respectively. Ranges are presented for each air mass type due to differing assumptions. This background range is considerably lower than the present value of 50% for the 6 – 8-km altitude range, but the convectively influenced CH_4 production contribution spans the 44% value determined here. For the 10-11-km range, Stickler et al. determined production percentages from CH_4 of 35% to 53% and 31% to 47%, respectively, for background and convectively influenced air, and this is in reasonable accord with present values of 50% and 34% for corresponding air mass types in the 10-12-km range. The next highest contribution in the Stickler et al. study is methanol followed by MHP for both background and perturbed air masses. This order is reversed in most cases in the present study. The production percentages for these two species are generally similar in both studies with the largest difference being ~ 14% for methanol at the lowest altitudes in the UT for the background case (22% for background conditions in Stickler et al. compared to 8% here) and ~ 12% MHP at the highest altitudes for the

background case (13% in Stickler et al. compared to 0.6% here). Similar to the present study, the UT CH_2O production contributions from other species such as acetaldehyde, PAN, and acetone in the Stickler et al study were all minor components compared to CH_4, methanol, and MHP.

The Stickler et al. study comes to the same conclusion as the present study regarding the importance of the transport of CH_2O precursors to the UT and the enhanced photochemical activity from NO due to lightning. However, a comparison of the total CH_2O production rates between the two studies indicates significantly enhanced photochemical activity at the highest altitudes over Europe compared to North America. For example, the Stickler et al study (10-11-km) reports CH_2O production rates of 3 x 10^5 and 1.2 x 10^6 molecules cm^{-3} s^{-1} for background and convective air, respectively, and this compares to significantly smaller median values of 1.5 x 10^5 and 3.4 x 10^5 molecules cm^{-3} s^{-1} for the 10-12-km range of the present study. There are many potential reasons for this difference which need to be further investigated.

6. CH_2O Measurement-Model Ratios in the UT versus NO and Relationship to HO_2 Ratios

As noted throughout this paper, the production rate for CH_2O is dramatically affected by NO, with the largest measurement-model differences occurring at the highest NO mixing ratios. The modeling study by Wang and Prinn [2000] reveals a doubling in the CH_2O production rate in the presence of lightning in the mid-troposphere due to an enhancement in the reaction between CH_3O_2 and NO. To further investigate the correlation between CH_2O and NO in this study, Fig. 10 plots the dependence of the (TDLAS/Box Model) ratio as a function of NO for the 3 different altitude bins in the UT. The same 1188 comparison points employed throughout (where there are measurements and box model results in the UT and where the latter employs measurements of MHP as a constraint) were used to generate this plot. Here we plot the binned median and

average measurement/model ratios as a function of NO (median NO for the median ratio and average NO for the average ratio). Also shown are the individual ratio measurements.

Linear fits of the measurement/model ratios (shown by the dark solid lines) are given with altitude bin. The first point in the 10 -12 km bin was excluded from this fit due to the sparseness of the data (N = 3 in the bin). The average number of comparisons for the other bins was 16. As can be seen by the linear fits, there is an increasing trend in the measurement/model ratio with NO that becomes apparent in the highest altitude bin where the NO mixing ratios are the highest. Discrepancies become readily apparent at NO mixing ratios greater than 1000-pptv. In the 6-8 km bin there is no trend and no data with NO > 1000-pptv. By contrast, in the 10 – 12 km altitude range a number of comparisons have NO > 1000-pptv; at the highest NO mixing ratio (bin median 4137-pptv) in this altitude range, the median CH_2O bin measurement/model ratio is 3.9. These observations are consistent with our previous discussions regarding the largest measurement-model discrepancies in the UT, which are found in the 10 – 12 km altitude bin. These observations imply one or a combination of the following: 1) reactions between CH_3O_2 and NO in the model are too slow compared to reality in the UT; 2) there are additional reactions that produce CH_2O in the atmosphere involving NO, which are not currently represented in the box model; 3) there are additional unknown CH_2O hydrocarbon precursors not in the box model during convection in the presence of high NO; 4) the modeled OH values are significantly lower than actual mixing ratios; 5) the CH_2O sink terms in the model (2 photolysis and 1 OH reaction channel) are too fast compared to reality in the UT; and/or 6) heterogeneous formation of CH_2O from methanol in clouds [Tabazadeh et al., 2004]. We will discuss each possibility below.

However, depending upon the CH_2O precursor type, lightning-enhanced NO may not in all cases yield elevated CH_2O production. As shown in Figure 3, convection of methanol and MHP

are not affected by NO for gas phase reactions, unless the back conversion of MHP to CH_3O_2 ($CH_3OOH + OH \rightarrow CH_3O_2 + HO_2$) dominates the decomposition of MHP in producing CH_2O.

It is important to note that measurement-model comparisons of HO_2 in the UT by Ren et al. [2007] during INTEX-NA show a very similar trend with NO above 8-km as our CH_2O comparisons in Fig. 10. This is reasonable since HO_2 is produced in two of the CH_2O decomposition channels as well as the hydrogen abstraction step from the CH_3O radical by O_2 during the production of CH_2O (Fig. 3). This suggests real atmospheric processing and not instrument artifacts as the cause of the trends. Based upon median values for CH_2O photolysis frequencies and reaction with OH above 8-km during INTEX-NA, we expect 0.8 HO_2 radicals formed for every CH_2O decomposition. Although inclusion of this CH_2O source in the HO_2 calculations (i.e., constraining the HO_2 calculation with measured CH_2O) reduces the HO_2 measurement/model discrepancy with NO above 8-km from a value of ~ 3.8 to 3.0 at the highest NO_x values, it is clear that additional sources of HO_2 and CH_2O are simultaneously needed in the box model. Since every reaction between CH_3O_2 and NO would simultaneously yield 1.8 HO_2 radicals for every CH_2O molecule formed (1 from $CH_3O + O_2$, and 0.8 from CH_2O decomposition), one explanation is that such additional source(s) primarily must flow through the CH_3O_2 + NO channel rather than from direct CH_2O emission sources. Reconciling the HO_2 discrepancy by increasing CH_2O photolysis rates has been discounted by Ren et al. [2007]; these researchers point out that it is quite unlikely that the photolysis frequencies are in error by the required factors of 4 to 6. Such errors, moreover, would further exacerbate the CH_2O discrepancy unless simultaneously accompanied by substantial increases in CH_2O production rates. Although reactions between OH and methanol add another HO_2, this channel is NO independent.

To examine the model deficit for both CH_2O and HO_2 as a function of NO, we plot in Fig. 11 the relationship between median HO_2 (measurement/model) and CH_2O (measurement/model) ratios for various binned values of NO calculated in the 8-12 km range. The original HO_2 data in the database was corrected by a factor of 1.64 to account for a calibration error discovered after the mission. Only data are shown where there are CH_2O measurement-model comparisons and where MHP is used in the model constraint. The solid line is linear fit of the data for NO values < 1500-pptv (N = 11). The anomalously low point at a CH_2O ratio of 1.5 was not included in this fit due to sparseness in the data in this bin (the same excluded data of Fig. 10 at very low NO values). As can be seen, the discrepancy for HO_2 is highly correlated with that for CH_2O when binned by NO (for NO median < 1500-pptv, slope = 3.0, $r^2 = 0.76$). As can be seen by the inset, binned NO values higher than 1500-pptv yield significantly larger HO_2 discrepancies relative to CH_2O, perhaps indicating a regime where HO_x is directly formed without CH_2O. The slope of 3.0 in Fig. 11 is a factor of 1.6 times the expected HO_2 per CH_2O relationship associated with CH_3O_2 + NO reactions discussed above. This comparison, however, is very simplistic since it does not take into account recycling of OH to HO_2 (other than the CH_2O decomposition with OH), the possibility that many HO_2 radicals can be generated in multiple steps from hydrocarbon decompositions, and the loss of HO_2 from HO_2 + HO_2 recombination.

It is interesting to note that the highest discrepancies for both CH_2O and HO_2 above 1000-pptv NO are also associated with the highest ultrafine condensation nuclei (UCN) values, aerosols with diameters as small as 3-nm. High UCN number densities generally reflect new particle formation. In the outflow of clouds, UCN values are often elevated due to fresh sulfuric acid production from SO_2 outflow, which reacts with enhanced OH caused by the elevated NO. Therefore, the apparent correlation in the discrepancies with UCN may be coincidental since the

highest UCN values are also associated with the highest NO values from the mechanism just described. In fact, it is difficult to find cases where NO levels are high and the UCN are less than their median UT values. Even at NO mixing ratios less than 1000-pptv, UCN and NO are still correlated, making it difficult to assign the prime contributor of the CH_2O and HO_2 discrepancies. However, a plot of the CH_2O discrepancy versus NO and colored by UCN (not shown) suggests that NO appears to be the more important factor. Section 8 will further explore one specific example where NO and UCN number densities are elevated.

7. Case Studies of UT Convection

While the CH_2O measurements and box model relationships previously discussed give us an overview of UT CH_2O perturbations over continental North America and the North Atlantic Ocean during summer months due to convection, this analysis does little to show our understanding and limitations in such understanding during individual perturbation events. Thus we now compare and contrast in this section three different convective cases in the UT: one involving convection of a mixed anthropogenic and biogenic plume, a second involving convection of an anthropogenic plume, and a third involving convection of well aged air with recent large NO inputs from lightning. All three cases will exemplify the CH_2O and HO_2 discrepancies with NO discussed in the previous section.

Figure 12, which displays the first case over the Maine-New Brunswick border at 9.1-km on August 11, 2004, reveals good TDLAS-box model agreement in CH_2O for two of three large excursions during this flight leg. The shaded regions indicate when the DC-8 was sampling in non-clear regions, which for times around 12:20 represent sampling in clouds. This figure also shows those box model points where measurements of MHP are available and used in the model (100% in this case).

Based upon elevated CO, SO_2, UCN, and MHP, as examples, the entire flight leg of Fig. 12 indicates convection of anthropogenic pollutants. However, an observed depression in CO_2 also suggests some biogenic origin to the convection from photosynthetic uptake. Since this process occurs during daylight hours, and the sampling time starts at 7:15 AM (local time), the contact with the biosphere must have originated at least 12-hours prior to sampling. Analysis using FLEXPART indicates contact with the biosphere several days prior to sampling. Based upon the meteorological analysis by Fuelberg et al. [2006] and the NO_x/HNO_3 ratios by Bertram et al. [2007], the convection and lightning influences were very recent in origin (0 to 10 hours for both). Based upon the 4 fire indicators discussed previously, this plume does not show any evidence of fire influence. Collectively, all the indicators above indicated a mixed biogenic/anthropogenic plume that was well aged but the convection and lightning influences were very recent.

The ratio between heated to un-heated condensation nuclei number densities, which was less than 0.1 in all cases, indicated a well-aged non-refractory plume. This ratio was measured with the same condensation nuclei instrument upon heating the inlet to 300 °C relative to an un-heated inlet. High ratios indicate a large number density of refractory species, which are typically dominated by soot, fly ash and generally indicative of pollution. The benzene to toluene ratios also indicated a well aged plume of 22 to 35-hours old, as determined using the approach given by Colomb et al. [2006]. Although the exact plume age from this approach is somewhat uncertain, the plume age is certainly much longer than typical CH_2O lifetimes.

Thus, one would expect elevated UT measurements and box model results for CH_2O, and given the age of the plume, these two results should agree, except possibly where NO is very large. Figure 12 panel (a) shows the resulting comparison between TDLAS CH_2O measurements,

box model results, and modeled NO. The random uncertainty limits (at the 2σ level) for both are also shown with each data point. As can be seen, the measurements and model results are in reasonable agreement (with a few exceptions) within the combined random uncertainties for the first two peaks (peak 1 at 12:20 – 12:26, peak 2 at 12:35 – 12:39, peak 3 at 12:46 – 12:48) but the model underestimates the observations by 286-pptv for the 3rd peak (measurement/model ratio = 1.69). Based upon the model production rates, MHP dominates the production of CH_2O in this plume (43 to 47% of the total CH_2O production) and its temporal profile largely dictates the temporal profile of the box model calculated CH_2O throughout Fig. 12.

During the 1st peak there are 4 measurements and box model determinations for comparison, and all 4 are in agreement within the mutual precision estimates. During the 2nd peak in Fig. 12 the modeled NO reached a high value of 1393-pptv at 12:36. The CH_2O and HO_2 measurement/model ratios here are 1.1 and 2.1, respectively. Based on the discussions of the previous section one would expect a significantly larger CH_2O ratio of ~ 1.8. However, since the MHP production percentage of CH_2O is still high here (43%), one would expect a much reduced NO affect on CH_2O, as is apparently the case. However, this is not consistent with the last two points in the 2nd peak (at 12:37 and 12:39) and the two points during the 3rd peak (12:47 and 12:48). Here both the CH_2O (measurement/model ratios of 1.3 to 1.7) and HO_2 (measurement/model ratios of 2.8 to 3.9) discrepancies are again present. In both cases, the MHP CH_2O production percentage is still high (36% to 45%), thus implying efficient production of CH_2O from CH_3O_2 at high NO.

Clearly the varying behavior of Fig. 12 points to major gaps in our understanding. In addition to NO, the only species that changes significantly between the 1st and 3rd peaks is H_2O; the median H_2O mixing ratio dropped by a factor of 2.5 from peak 1 to peak 3 and the relative

humidity dropped from 95% to 78%. In addition, the sampled air changed from largely cloudy conditions to clear conditions between peaks 1 and 3, as shown. The second peak was largely in clear air with the exception of one small time interval in haze and the median H_2O vapor and relative humidity were similar in magnitude to the 3rd peak. It is interesting to note that the relative enhancements in UCN (peak- local background value/local background value) are very similar to those for the measured CH_2O mixing ratios for all three peaks, reinforcing our discussion above that CH_2O enhancements may be related to similar processes as those responsible for the UCN formation. However, as the NO profiles are also similar in shape these two effects cannot be separated.

Figure 13 shows a second convective case in the UT at 10-km employing data acquired on August 6, 2004 out over the North Atlantic Ocean about 100 miles off the United States coast spanning a track east of Cape Cod to east of Delaware. As with the previous example, SO_2 was elevated. Since the sampling occurred early in the morning (around 8 am local time), the convection most likely occurred during the dark. Also like the previous case, there is no evidence of fire exposure, but unlike the previous case there is no evidence for recent biogenic exposure (CO_2 levels not depressed). Hence the plume shown in Fig. 13 was anthropogenic in origin.

Figure 13a shows those box model points where measurements of MHP are available and used in the model. As can be seen, in contrast to Fig. 12a, measurements of MHP were not available for many of the modeled CH_2O points and this dramatically affected the modeled CH_2O results as discussed previously. Comparisons based upon calculated MHP significantly underestimated the observations and produced an apparent oscillation in the model results (13:10 and 13:15) whenever modeled values of MHP were interspersed among time periods employing measured MHP values.

This figure highlights two time periods: 12:49 – 12:53 and 13:04 – 13:21. Convection and lightning occurred ~ 1 hour and ~ 7 to 9 hours before sampling, respectively, for the first period, and 3 to 5 hours and 0 to 3 hours prior to sampling, respectively for the second period. During the first period the median measurement-model difference was 434-pptv and produced a median ratio of 2.1. The largest production contribution from the model was CH_4 (35%) followed by MHP (22%) during this period. As can be seen, the modeled NO produced a peak at 12:51, right where the measured CH_2O peaked. The HO_2 measurement/model ratio for this point averaged 3.8. As in Fig. 12, there was a large spike in UCN measurements that mirrored the shape of the TDLAS CH_2O measurements. Underestimation of OH in the model cannot be the cause of the CH_2O underprediction here since the corrected OH measurements and model values were within 15% of one another.

During the second time period there is no formal peak evident, but an extended comparison period (N = 14 where measurements of MHP were used in the model). The median CH_2O measurement-model difference was 42-pptv and the median measurement/model ratio was 1.1 for these points. The median NO and HO_2 measurement/model ratio over this time period was 480-pptv and 1.1, respectively. The model indicated that MHP had the largest production contribution (53%) followed by CH_4 (19%) during this second time period. This explains the large model sensitivity to the MHP input employed in the CH_2O calculation; apparently convection of MHP takes on a significant role here that cannot be modeled adequately by standard HO_x-NO_x-CH_4 chemistry without MHP measurements used to constrain the model. The box model (with MHP measurements employed as a model constraint) in Fig. 13 captures the CH_2O observations during the convection in all but four of the points during the 2nd period.

Thus, like Fig. 12, the convection in Fig. 13 shows time periods where the atmospheric processes are reasonably well understood and time periods where this is not the case, and both are related to NO mixing ratios as well as the HO_2 measurement/model relationship.

Figure 14 shows a third case study example. Measurements during this flight leg were acquired at 10.7-km over South Carolina on July 8, 2004. This shows an example involving convection of well aged air with recent large NO inputs from lightning. Back trajectories indicated the air passed over the south eastern United States but remained at altitude between 7 and 10.7-km over the past two days. As can be seen in Fig. 14, UCN and NO were both significantly elevated (right hand axes of Fig. 14) at the start of this leg. Both peaked at 20:50 where the CH_2O and HO_2 displayed their greatest measurement/model discrepancies (CH_2O measurement/model = 3.4 and HO_2 measurement/model = 16.0). In this example the MHP values were low enough (median = 44) that it made no difference whether or not measured or modeled MHP was employed in the CH_2O calculation. As the NO dropped, the CH_2O measurements came into agreement with the model. For HO_2, the measurement/model ratio was still significantly greater than 1, even for NO values < 1000-pptv. This again shows the higher NO sensitivity of HO_2 compared to CH_2O, and may reflect the importance of RO_2 + NO reactions. In contrast to the CH_2O profile, where the measurements declined by over 200-pptv while the modeled values were relatively constant, the HO_2 measurement decline was ~ 2.6-pptv and the model increased by approximately the same amount.

At the peak (20:50), many of the tracers indicated in Table 3 were at or near their 10-12-km median values, with a few exceptions (propane and the butanes were 2 to 3 times their median values, are examples). Anthropogenic combustion tracers like CO, ethyne, and SO_2 were all less than their 10-12-km median values. At times around 20:50, the Fuelberg analysis indicated a

time since convection of ~ 3 hours but lightning influence within 1 hour of sampling. Based on the analysis of Eq. 4 using an instantaneous CH_2O lifetime of 1.5-hours, direct convection of CH_2O should not be important here.

8. Possible Causes of the UT CH_2O and HO_2 Discrepancies

During all 3 case studies for the constant altitude portions of the measurement-model comparisons, changes in ambient temperatures and pressures were all less than 0.5% (0.8-K, and 0.3-mb). Thus the variable measurement-model agreement during these flight legs implies that temperature and pressure related rate constant and photolysis frequency errors as well as branching ratios errors (potential cause #5) are not the cause of the discrepancies. Errors in any of these parameters would not yield measurement-model agreement during parts of the flight legs and disagreement during other parts. Likewise, this logic also rules out errors in the rate constant for CH_3O_2 + NO (potential cause #1) as well as additional reactions that produce CH_2O and HO_2 in the atmosphere involving NO which are not currently represented in box models (potential cause #2), unless heterogeneous production on aerosols, which is time coincident with the elevated NO becomes important. The 4th potential cause, significantly lower modeled OH mixing ratios than those measured can be ruled out in two of the three cases; here modeled OH values were higher than those measured, even after a correction of the initial measurements by the factor of 1.64. In the third case, the CH_2O measurement/model ratio at 20:50 in Fig. 14 is 3.5 using modeled OH. This ratio reduces to a value of ~ 2.1 when we employ measured OH values corrected by the factor of 1.64. Hence, lower modeled OH mixing ratios than those present in the UT cannot explain the CH_2O discrepancies in the three case studies.

This leaves us with two main possibilities for the observed discrepancies: unmeasured hydrocarbon precursors (potential cause #3), and/or heterogeneous formation of CH_2O on

aerosols and/or in clouds. In Section 6 we discussed the possibility that in addition to elevated NO, elevated ultrafine condensation nuclei may also play some role in causing the observed CH_2O and HO_2 measurement-model discrepancies in the UT. However, both the surface area and volume of UCNs are orders of magnitude too low for heterogeneous reactions to be important here. Such reactions, therefore, would require surface areas such as those found in clouds. The heterogeneous processing of methanol to form CH_2O in certain clouds (potential cause #6) is one such possibility, and this has been discussed by Tabazadeh et al. [2004]. These researchers presented evidence based upon Fourier Transform IR measurements to support the importance of this mechanism in clouds that have encountered biomass burning plumes. One possible mechanism postulated, involved cloud uptake of NO_2 and the formation of HO_2, both of which are consistent with the observations of this study. These authors further raised the possibility of similar processes occurring on more pristine clouds that have not encountered biomass plumes, as would be needed to explain the present observations; as discussed previously, biomass burning influence was not evident in the discrepancies observed here.

To explore the possibility of such heterogeneous conversion of methanol to CH_2O in clouds, we further examined the three case studies presented in Fig. 12 to 14. Of the three, the total cloud surface area density was only appreciable for the measurements around 12:20 of Fig. 12 on August 11, 2004. Here the DC-8 was sampling in clouds with a total surface area density, S, of 0.0016 $cm^2\ cm^{-3}$ for cloud particles in the 0.3 to 1550-μm size range. We estimate the magnitude of potential heterogeneous production of CH_2O in this cloud utilizing the heterogeneous rate constant and expressions derived by Tabazadeh et al. [2004]. We assume that the cloud surface area size distribution was equivalent in the two studies and that the Tabazadeh heterogeneous normalized rate constant in smoke/cloud plumes for reactions involving NO_2 ($k_{het} = 4.3 \times 10^{-13}$

$cm^3\ s^{-1}$) was also appropriate for the pristine clouds of the present study. The present calculations are therefore probably an upper limit. The Fuelberg et al. convective analysis indicated that the air sampled at 12:20 was exposed to fresh convection for the past 21-hours, and IR satellite imagery coupled with back trajectories indicated that this air was in clouds for at least 8-hours prior to sampling. Assuming a surface area density of 0.0016 $cm^2\ cm^{-3}$ for the entire cloud exposure, and a processing time of 8-hours, we estimate the resulting heterogeneous CH_2O production from the expression derived by Tabazadeh et al. [2004]:

$$[CH_2O]_{het} = [\text{Processing Time}][k_{het}][S][NO_2][CH_3OH] \quad (5)$$

Employing NO_2 and methanol mixing ratios of 315-pptv and 2741-pptv, respectively, measured at 12:20 (M = 1.1 x 10^{19} molecules cm^{-3}), together with values of S and k_{het} given above, we calculate a CH_2O mixing ratio of 184-pptv (23-pptv hr^{-1}) due to heterogeneous conversion of methanol with NO_2 in pristine clouds. Under this scenario, we should have observed a CH_2O measurement-model discrepancy of +184-pptv at 12:20, since the box model does not include this process. The actual measurement-model discrepancy at 12:20 was -110-pptv and averaged 51 ± 106-pptv for the entire non-clear period in Fig. 12 around 12:20. The largest discrepancies observed in Fig. 12 occurred at 12:47 and 12:48 (+277-pptv), ~ 6-hours transport time after the cloud exposure at 12:20. As this is ~ 4 CH_2O lifetimes, any heterogeneous cloud processing should have recovered by the time of sampling at 12:47 and 12:48. Given these facts, it is therefore highly unlikely that heterogeneous conversion of methanol on pristine clouds to form CH_2O in the presence of elevated NO_x in the UT is important in this study.

The final possible mechanism for the observed discrepancies in the presence of elevated NO involves gas-phase reactions of unmeasured hydrocarbons. If important, the NO-dependent

discrepancies imply that their decomposition must proceed through RO_2 radicals. Steady-state calculations were carried out to assess the magnitude of the potential missing hydrocarbon sources needed to reconcile the CH_2O measurements and modeled values for NO mixing ratios higher than 2000-pptv in 10-12 km altitude range that proceed through RO_2 radicals. A missing relatively long-lived hydrocarbon with the same reactivity as propane (k_{OH} = 9.3 x 10^{-13}) would need to be present at mixing ratios of approximately 2-ppbv. This is consistent with the abundance determined by Ren et al. [2007] needed to reconcile OH and HO_2 mixing ratios above 10-km, after scaling their assumed OH reactivity of 2 x 10^{-11} cm^3 $molecule^{-1}$ s^{-1} to the propane reactivity. Faster reacting alkenes with the same reactivity as ethene and isoprene (k_{OH} = 6.6 x 10^{-12} and 9.7 x 10^{-11}) would need to be present at much lower mixing ratios of approximately 216-pptv, and 32-pptv, respectively, to reconcile the CH_2O discrepancy. Although both types of missing hydrocarbons are possible, the order of magnitude lower mixing ratio for the faster reacting hydrocarbons appears to be the more realistic scenario. However, a large number of undetected slower reacting hydrocarbons at very low individual mixing ratios could also be the cause for the CH_2O discrepancy.

9. Summary and Conclusions

Measurements of CH_2O from a tunable diode laser absorption spectrometer (TDLAS) were acquired onboard the NASA DC-8 during the summer 2004 INTEX-NA campaign. These measurements were compared to box model calculations to further test our understanding of hydrocarbon oxidation chemistry and convective transport in the upper troposphere (6-12-km) over continental North America and the North Atlantic Ocean.

Various tracers were used together with back trajectories and other tools to arrive at a set of 77 background air mass time periods in the UT where the air was not influenced by the boundary

layer or residual layers for at least the past 24-hours. Ninety-nine percent of the composite CH_2O measurements from the TDLAS and CENZ systems onboard the DC-8 as well as the box model results during these time periods spanned the range between -56 to 165-pptv, and this defined our background non-perturbed UT CH_2O range over North America and the North Atlantic Ocean. These three data sets indicated that a substantial fraction of the CH_2O measurements and model results in the UT (38% to 46%) over North America and the North Atlantic surpassed the 165-pptv background upper limit during the summer of 2004 due to convection.

We used the box model results to further indicate the CH_2O precursors responsible for CH_2O production in the UT. In general CH_2O production from CH_4 was found to be the dominant source term, even in perturbed air masses. This was followed by production from MHP (CH_3OOH), methanol, PAN type compounds, and ketones, in descending order of their contribution. However, a number of convection cases were also identified where MHP and/or methanol played the dominant role in producing UT CH_2O.

Two different approaches were employed to estimate a lower limit for the percentage of time that such elevated UT CH_2O observations were associated with enhanced production from CH_2O precursors, including enhanced production due to enhanced NO from lightning and other causes, rather than from direct convection of boundary layer CH_2O. In the case of the former, a time-dependent box model indicated enhanced UT CH_2O levels, and hence radical production, lasting as long as one or more weeks. This compared to elevated UT CH_2O levels lasting approximately only one day in the case of direct boundary injection. Thus, understanding the exact mechanism responsible for elevated CH_2O in the UT is important for understanding its integrated influence and the extent of influence downwind of convection. The two different determinations indicated that at least 66% to 73% of the perturbed CH_2O observations (values > 165-pptv) in the UT by

TDLAS were caused by enhanced production from CH_2O precursors, including enhancements from lightning perturbed NO. For the remaining 27% to 34% of the time our perturbed UT observations can be ascribed to direct CH_2O convection and/or convection of CH_2O precursors. At present there is no way to pull these two effects apart, and thus CH_2O precursors may be playing an even larger role in the UT.

The median measurement/model ratio in the UT was 0.91 when measurements of MHP were available to constrain the model. However, individual ratios exhibited a great deal of scatter with discrepancies as large as 20.8. In the UT, 56% of the measurement-model comparisons were within the combined random uncertainties and 62% were within the combined systematic uncertainty limits, even after restricting the model to time periods when measurements of MHP were available as a model constraint (N = 1188). A further comparison revealed that both measured and modeled CH_2O were both significantly elevated in the UT when sampling in non-clear conditions due to convection of pollution. This increase was more than a factor of 2 in the 10-12 km range compared to clear conditions. Nevertheless, the median point-by-point measurement/model ratios were still in agreement during these conditions, indicating that the box model faithfully captures the observations during most of the convective perturbations throughout the UT.

The CH_2O measurement-model agreement was also studied as a function of NO in the UT. In the 6-8-km bin, there essentially was no trend in the comparisons. By contrast, in the 10-12-km range there was a significant trend, which for the highest NO mixing ratio (bin median value of 4137-pptv), produced a median CH_2O measurement/model ratio of 3.9. It is important to note that Ren and colleagues observed a similar trend with NO in their measurement-model comparisons of HO_2 during the INTEX-NA study. The discrepancies in HO_2 and CH_2O

measurement/model ratios were highly correlated in the 8-12-km range at NO mixing ratios less than 1500-pptv. At higher mixing ratios the HO_2 discrepancy increased significantly faster than that of CH_2O. Since both CH_2O and HO_2 show similar trends with NO, it is highly unlikely that both instruments experienced similar instrument artifacts. We believe that the NO-dependent discrepancies for both gases are related and are most likely caused by unmeasured hydrocarbon precursors.

It is clear that more systematic studies of CH_2O and HO_x measurement-model relationships in the UT are needed as a function of NO, particularly in and around clouds, and in the presence of high UCN number densities and high methanol mixing ratios. Systematic measurements are also needed where the cloud hydrometer types are well-characterized. Studying the behavior of CH_2O during freezing nucleation processes, for example, would be of particular interest. As discussed by Barth et al. [2007], soluble gases like CH_2O could degas from cloud droplets as the solution starts to freeze. Such a process would act as an efficient mechanism in transporting boundary layer CH_2O to the UT.

Based on the results of this study, it is clear that understanding radical chemistry in the UT requires reconciling CH_2O measurement-model discrepancies in addition to those for HO_2. This is particularly true since enhanced photochemical production of CH_2O in the UT in the presence of convection and lightning was shown to be prevalent over a large fraction of our observations. Perturbed CH_2O in the UT over North America and the North Atlantic Ocean is far more important during summer months than previously recognized.

Acknowledgements: The National Center for Atmospheric Research is operated by the University Corporation for Atmospheric Research under the sponsorship of the National Science

Foundation. This research was supported by funds from the National Aeronautics and Space Administration's Global Tropospheric Experiment. The authors specifically wish to acknowledge the NASA DC-8 staff and crew for all their valuable support and assistance and Mary Barth, Chris Cantrell, and John Orlando at NCAR for valuable discussions. The GEOS-Chem model is managed by the Atmospheric Chemistry Modeling group at Harvard University with support from the NASA Atmospheric Chemistry Modeling and Analysis Program.

References

Barth, M.C., S.-W. Kim, W.C. Skamarock, A.L. Stuart, K.E. Pickering, and L.E. Ott, Simulations of the redistribution of formaldehyde, formic acid, and peroxides in the July 10, 1996 STERAO deep convection storm, J. Geophys. Res., in press, 2007.

Bertram, T.H., et al., Direct measurements of the convective recycling of the upper troposphere, in press, Science, 2007.

Brune, W.H., et al., Airborne in-Situ OH and HO_2 observations in the cloud-free troposphere and lower stratosphere during SUCCESS, Geophys. Res. Lett., **25** (10), 1701 – 1704, 1998.

Cohan, D.S. M.G. Schultz, D.J. Jacob, B.G. Heikes, and D.R. Blake, Convective injection and photochemical decay of peroxides in the tropical upper troposphere: methyl iodide as a tracer of marine convection, J. Geophys. Res., **104**, 5717 – 5724, 1999.

Colomb, A., J. Williams, J. Crowley, V. Gros, R. Hofmann, G. Salisbury, T. Klüpfel, R. Kormann, A. Strickler, C. Forster, and J. Lelieveld, Airborne measurements of trace organic species in the upper troposphere over Europe: the impact of deep convection, Environ. Chem., **3**, 244 – 259, doi: 10.1071/EN06020, 2006.

Crawford, J. H., et al. Assessment of upper tropospheric HO_x sources over the tropical Pacific based on NASA GTE/PEM data: net effect on HO_x and other photochemical parameters, J. Geophys. Res., **104**, 16,255-16,273, 1999.

Dasgupta, P.K., J. Li, G. Zhang, W.T. Luke, W.A. McClenny, J. Stutz, and A. Fried, Summertime ambient formaldehyde in five U.S. metropolitan areas: Nashville, Atlanta, Houston, Philadelphia, and Tampa, Environ. Sci. Technol., **39**, 4767 – 4783, 2005.

Faloona, I., et al., Observations of HO_x and its relationship with NO_x in the upper troposphere during SONEX, J. Geophys. Res., **105**, (D3), 3771 – 3783, 2000.

Fried, A., Y.-N. Lee, G. Frost, B. Wert, B. Henry, J.R. Drummond, G. Hubler, and T. Jobson, Airborne CH_2O measurements over the North Atlantic during the 1997 NARE campaign: instrument comparisons and distributions, J. Geophys. Res., **107**, doi: 10.1029/2000JD000260, 2002.

Fried, A., et al., Airborne tunable diode laser measurements of formaldehyde during TRACE-P: distributions and box-model comparisons, J. Geophys. Res., **108** (D20), 8798, doi: 10.1029/2003JD003451, 2003.

Fried, A., et al., Formaldehyde over North America and the North Atlantic during the summer 2004 INTEX Campaign: Methods, Observed Distributions, and Measurement Box Model Comparisons, in preparation for submission to J. Geophys. Res., 2007.

Fuelberg, H.E., M.J. Porter, C.M. Kiley, and D. Morse, Meteorological conditions and anomalies during INTEX-NA, in press, J. Geophys. Res., 2006.

Jaeglé, L, et al., Observed OH and HO_2 in the upper troposphere suggest a major source from convective injection of peroxides, Geophys. Res. Lett., **24**(24), 3181 – 3184, 1997.

Jaeglé, L, D.J. Jacob, W.H. Brune, D. Tan, I.C. Faloona, A.J. Weinheimer, B.A. Ridley, T.L. Campos, and G.W. Sachse, Sources of HO_x and production of ozone in the upper troposphere over the United States, Geophys. Res., Lett., **25** (10), 1709 – 1712, 1998a.

Jaeglé, L, et al., Sources and chemistry of NO_x in the upper troposphere over the United States, Geophys. Res., Lett., **25** (10), 1705 – 1708, 1998b

Jaeglé, L, et al., Photochemistry of HO_x in the upper troposphere at northern midlatitudes, Geophys. Res., **105** (D3), 3877 –3892, 2000

Kleinman, L.I., P.H. Daum, Y.-N. Lee, L.J. Nunnermacker, S.R. Springston, J. Weinstein-Lloyd, and J. Rudolph, A comparative study of ozone production in five U.S. metropolitan areas, J. Geophys. Res., **110** (D2), D02301, doi: 10.1029/2004JD005096, 2005.

Kormann, R., H. Fischer, M. de Reus, M. Lawrence, Ch. Brühl, R. von Kuhlmann, R. Holzinger, J. Williams, J. Lelieveld, C. Warneke, J. De Gouw, J. Heland, H. Ziereis, and H. Schlager, Formaldehyde over the eastern Mediterranean during MINOS: comparison of airborne in-situ measurements with 3D-model results, Atmos. Chem. Phys., **3**, 851 – 861, 2003.

Lee, Y.-N, et al., Atmospheric chemistry and distribution of formaldehyde and several multioxygenated carbonyl compounds during the 1995 Nashville/Middle Tennessee ozone study, J. Geophys. Res., **103** (D17), 22,449 – 22,462, 1998.

Lelieveld, J., H. Berresheim, S. Borrmann, P.J. Crutzen, F.J. Dentener, H. Fischer, J. Feichter, P.J. Flatau, et al., Global pollution crossroads over the Mediterranean, Science, 298, 794 - 799, doi: 10.1126/SCIENCE.1075457, 2002.

Millet, D.B. D. J. Jacob,, S. Turquety, R.C. Hudman, S. Wu, A. Fried, J. Walega, B.G. Heikes, D. R. Blake, H.B. Singh, B.E. Anderson, and A.D. Clarke, Formaldehyde distribution over North America: implications for satellite retrievals of formaldehyde columns and isoprene emission, J. Geophys. Res., **111**, doi:10.1029/2005JD006853, 2006.

Müller, J-F, and G. Brasseur, Sources of upper tropospheric HO_x: a 3-dimensional study, J. Geophys. Res., **104** (D1), 1705 – 1715, 1999.

Nunnermacker, L.J., J. Weinstein-Lloyd, L. Kleinman, P.H. Daum, Y.-N. Lee, S.R. Springston, P. Klotz, L. Newman, G. Neuroth, and P. Hyde, Ground-based and aircraft measurements of trace gases in Phoenix, Arizona (1998), Atmos. Environ, **38** (29), 4941 – 4956, 2004.

Prather, M.J., and D.J. Jacob, A persistent imbalance in HO_x and NO_x photochemistry of the upper troposphere driven by deep tropical convection, Geophys. Res. Lett., **24** (24), 3189 – 3192, 1997.

Ravetta, F. et al., Experimental evidence for the importance of convected methylhydroperoxide as a source of hydrogen oxide (HO_x) radicals in the tropical upper troposphere, J. Geophys. Res., **106**, 32,709 – 32,716, 2001.

Ren, X., et al., HO_x Observations and Model Comparisons during INTEX-A 2004, submitted to J. Geophys. Res., 2007.

Singh, H.B., W. Brune, J. Crawford, and D. Jacob, Overview of the summer 2004 Intercontinental Chemical Transport Experiment-North America (INTEX-A), in press, J. Geophys. Res., 2007.

Snow, J., B.G. Heikes, H. Shen, D. O'Sullivan, A. Fried, and J. Walega, Hydrogen peroxide, methyl hydroperoxide, and formaldehyde over North America and the North Atlantic, in press, J. Geophys. Res., 2006.

Stickler, A., H. Fischer, J. Williams, M. De Reus, R. Sander, M.G. Lawrence, J.N. Crowley, and J. Lelieveld, Influence of summertime deep convection on formaldehyde in the middle and upper troposphere over Europe, J. Geophys. Res., **111** (D14308), doi: 10.1029/2005JD007001, 2006.

Stohl, A., M. Hittenberger, and G. Wotawa, Validation of the Lagrangian particle dispersion model FLEXPART against large scale tracer experiments, Atmos. Environ., **32**, 4245 – 4264, 1998.

Tabazadeh, A., R.J. Yokelson, H.B. Singh, P.V. Hobbs, J.H. Crawford, and L.T. Iraci, Heterogeneous chemistry involving methanol in tropospheric clouds, Geophys. Res. Lett., **31,** doi: 10.1029/2003GL018775, 2004.

Wang, Y, and R.G. Prinn, On the roles of deep convective clouds in tropospheric chemistry, J. Geophys. Res., **105**, 22,269 – 22,297, 2000.

Wennberg, P.O., et al., Hydrogen radicals, nitrogen radicals, and the production of O_3 in the upper troposphere, Science, **279**, 49 – 53, 1998.

Wert, B.P., M. Trainer, A. Fried, T.B. Ryerson, B. Henry, W. Potter, W.M. Angevine, E. Atlas, S.G. Donnelly, F.C. Fehsenfeld, G.J. Frost, P.D. Goldan, A. Hansel, J.S. Holloway, G. Hubler, W.C. Kuster, D.K. Nicks Jr., J.A. Neuman, D.D. Parrish, S. Schauffler, J. Stutz, D.T. Sueper, C. Wiedinmyer, and A. Wisthaler, Signatures of terminal alkene oxidation in airborne formaldehyde measurements during TexAQS 2000, J. Geophys. Res., **108** (D3), 4104, doi: 10.1029/2002JD002502, 2003.

Tables

Table 1a: Median values (only when CH_2O measurements, model values, and measured MHP values are available for model input) for the indicated parameters under clear and non-clear (shaded rows) conditions for the pressure altitude range (Palt in km) under consideration. The species MHP and MeOH are CH_3OOH and Methanol, respectively. The convection time and lightning times are the times from the Fuelberg analysis before the DC-8 sampled the air mass in question. A time of 1 hour indicates the sampled air experienced the perturbation up to 1 hour before sampling. Most of the non-clear sampling occurred in haze and under intermediate conditions. Only 15% of the non-clear encounters involved at least 50% cloud coverage in the 6-12-km range.

Palt Range	[CH_4] ppmv	[MHP] pptv	[MeOH] pptv	[CO] ppbv	Convection Time (hr)	Lightning Time (hr)	CH_2O Lifetime (hr)
6 – 8	**1.794**	**209**	**1781**	**99**	**11**	**11**	**1.7**
6 – 8	**1.792**	**374**	**1691**	**97**	**6**	**5**	**2.8**
8 – 10	**1.791**	**124**	**1494**	**96**	**11**	**13**	**1.5**
8 – 10	**1.805**	**134**	**2516**	**117**	**3**	**13**	**1.5**
10 – 12	**1.778**	**94**	**731**	**94**	**12**	**12**	**1.5**
10 – 12	**1.819**	**178**	**2807**	**124**	**4**	**1**	**1.2**

Table 1b: Median point-by-point CH_2O measurement/box model ratios and associated median NO_x mixing ratios for the given pressure altitude range (Palt in km) under clear and non-clear (shaded rows) conditions. The CH_2O measurements are from the 1-minute TDLAS merge.

Palt Range (km)	**Median CH_2O (Measurement/Model)**	**Median [NO_x] (pptv)**
6 – 8	**0.85**	**142**
6 – 8	**0.79**	**159**
8 – 10	**0.91**	**427**
8 – 10	**1.01**	**340**
10 – 12	**0.97**	**667**
10 – 12	**1.11**	**671**

Table 2: Measurement/Model ratios in the 6-12-km pressure altitude range for all comparisons (N = 1642) and for comparisons where MHP measurements are available and used to constrain the model (N = 1188).

Parameter	(Meas/Model) All	(Meas/Model) with MHP
Avg ± 1 Std	1.2 ± 1.4	1.1 ± 1.4
0%	-1.5	-1.4
10%	0	0.07
25%	0.49	0.47
50%	0.94	0.91
75%	1.5	1.4
90%	2.6	2.3
100%	20.8	20.8

Table 3a: Primary species and their lowest 25 percentile mixing ratios in the UT (6 – 12 km) used to determine background conditions. All mixing ratios are in pptv with the exception of CH_4, CO, O_3, and UCN (ultra fine aerosol number density in the 3 – 10 nm size bins) which are in ppmv, ppbv, ppbv, and particles cm^{-3}, respectively. Measurements at their limit of detection (LOD) were included in this analysis by assigning the LOD for the mixing ratio.

Species Number	Species	Mixing Ratio
1	CH_4	1.779
2	Ethane	551
3	Ethene	3
4	Ethyne	62
5	Propane	66
6	Propene	3
7	i-Butane	3
8	n-Butane	7
9	Benzene	5
10	C_2Cl_4	2.5
11	CO	89
12	CO	83
13	Benzene	14
14	O_3	65*
15	UCN	579

Species 1 - 11: From Univ. California Irvine air collection/GC-MS system
Species 12: From the NASA Langley DACOM TDL system
Species 13: From the NASA Ames PANAK system
Species 14: From the NASA Langley FASTOZ Ozone system
Species 15: From the University of Hawaii aerosol system.

*The 65-ppbv value for O_3 was allowed to be exceeded for stratospheric legs.

Table 3b: Additional species and their lowest 25 percentile mixing ratios in the UT (6 – 12 km) used in helping to determine background conditions. All mixing ratios are in pptv except H_2O and CO_2 which are in ppmv. As in 3a, measurements at the LOD were set equal to the LOD.

Species Number	Species	Mixing Ratio
16	MHP	30
17	HCN	259
18	PAN	200
19	MEK	38
20	Methanol	753
21	Ethanol	20
22	CH_3CN	131
23	H_2O	148
24	CO_2	373.4
25	SO_2	5
26	OCS	443

Species 16: From URI CENZ system
Species 17-22: From the NASA Ames PANAK system
Species 23: From NASA Langley DLH system
Species 24: From NASA Langley NDIR system
Species 25: From GIT CIMS system
Species 26: From Univ. California Irvine air collection/GC-MS system

Table 4a: Statistics for time coincident CH_2O TDLAS and Box model results for the 6 – 12 km P_{alt} range for all locations during INTEX-NA. Background time periods (where Box model results are ≤ 165 pptv) are shown in light gray shaded rows while perturbed time periods (where Model > 165 pptv) are in darker shaded rows. All mixing ratios are in pptv and the standard deviations are indicated with the averages. In the 10-12 km range, 27 additional points were added to the perturbed periods where NO mixing ratios > 1000-pptv (see text for a description of the rational for this). This data set is based on the 1188 comparison points where MHP measurements are used in the model constraint.

	TDLAS			**Box Model**		
Palt. Range	**Average**	**Median**	**N**	**Average**	**Median**	**N**
6 - 8 km	**156 ± 205**	**104**	**153**	**119 ± 31**	**125**	**153**
6 – 8 km	**254 ± 202**	**211**	**314**	**264 ± 100**	**237**	**314**
8 – 10 km	**131 ± 178**	**90**	**237**	**108 ± 37**	**113**	**237**
8 – 10 km	**268 ± 208**	**212**	**245**	**250 ± 73**	**230**	**245**
10 – 12 km	**95 ± 114**	**68**	**170**	**99 ± 37**	**99**	**170**
10 – 12 km	**337 ± 212**	**293**	**69**	**230 ± 150**	**190**	**69**

Table 4b: Point-by-point differences (TDLAS-Box Model) and Median TDLAS/Box Model ratios for the P_{alt} ranges and air mass categories of Table 4a. All mixing ratios are in pptv and the standard deviations are indicated with the averages. Also shown are the median NO_x mixing ratios for each category from the steady-state calculated NO and measurements of NO_2.

Palt. Range	**Average**	**Median**	**TDLAS/Model**	**[NO_x]**
6 - 8 km	**38 ± 200**	**-14**	**0.89**	**68**
6 – 8 km	**-10 ± 173**	**-31**	**0.86**	**103**
8 – 10 km	**24 ± 172**	**-11**	**0.92**	**269**
8 – 10 km	**17 ± 186**	**-10**	**0.96**	**396**
10 – 12 km	**-3 ± 113**	**-24**	**0.72**	**548**
10 – 12 km	**107 ± 177**	**64**	**1.3**	**1391**

Table 4c: Median OH mixing ratios in pptv for background and perturbed air masses for the 3 altitude bins in the UT for the same data set (N=1188) in Tables 4a and 4b. The ratios for the perturbed to background medians are given by the Ratio term in the third column. The fourth column, labeled M, gives the median molecular number density in molecules cm^{-3} for the conditions specified.

Palt. Range	Median	Ratio	M
6 - 8 km	**0.174**		**1.19×10^{19}**
6 – 8 km	**0.215**	**1.2**	**1.20×10^{19}**
8 – 10 km	**0.301**		**9.16×10^{18}**
8 – 10 km	**0.389**	**1.3**	**9.42×10^{18}**
10 – 12 km	**0.390**		**7.82×10^{18}**
10 – 12 km	**0.599**	**1.5**	**7.88×10^{18}**

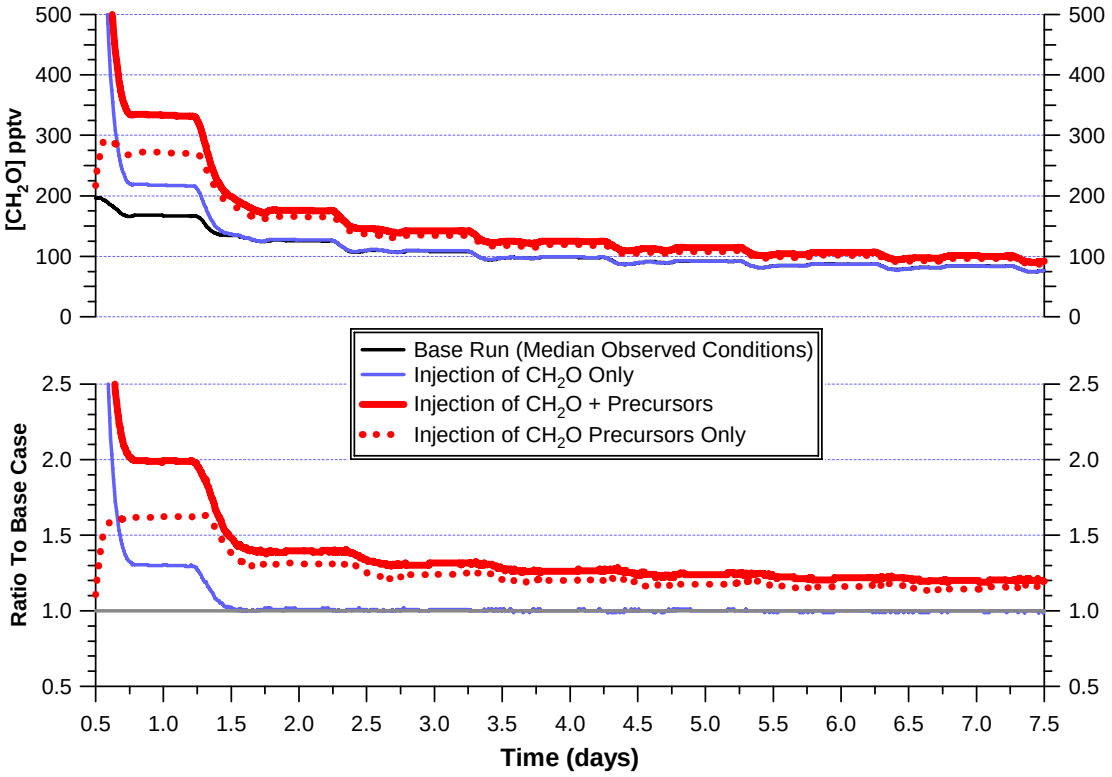

Figure 1

Figure 1: Box model runs for different scenarios at 9km. In the base run in all cases the model was run forward in a time-dependent mode for 7 days using observed median conditions and mixing ratios for 9 km (8.5 to 9.5 km) as the initial conditions. The time-dependent CH_2O mixing ratios were then calculated. The box model was then run using different injection scenarios starting at 12 noon based upon median mixing ratios from the boundary layer ($[CH_2O]$ = 2065 pptv, $[CH_4]$ = 1832 ppbv, [MHP] = 606 pptv, $[CH_3OH]$ = 3931 pptv, [Acetone] = 1808 pptv, [PAN] = 330 pptv). A median observed 9 km $[NO_x]$ mixing ratio of 345 pptv was input.

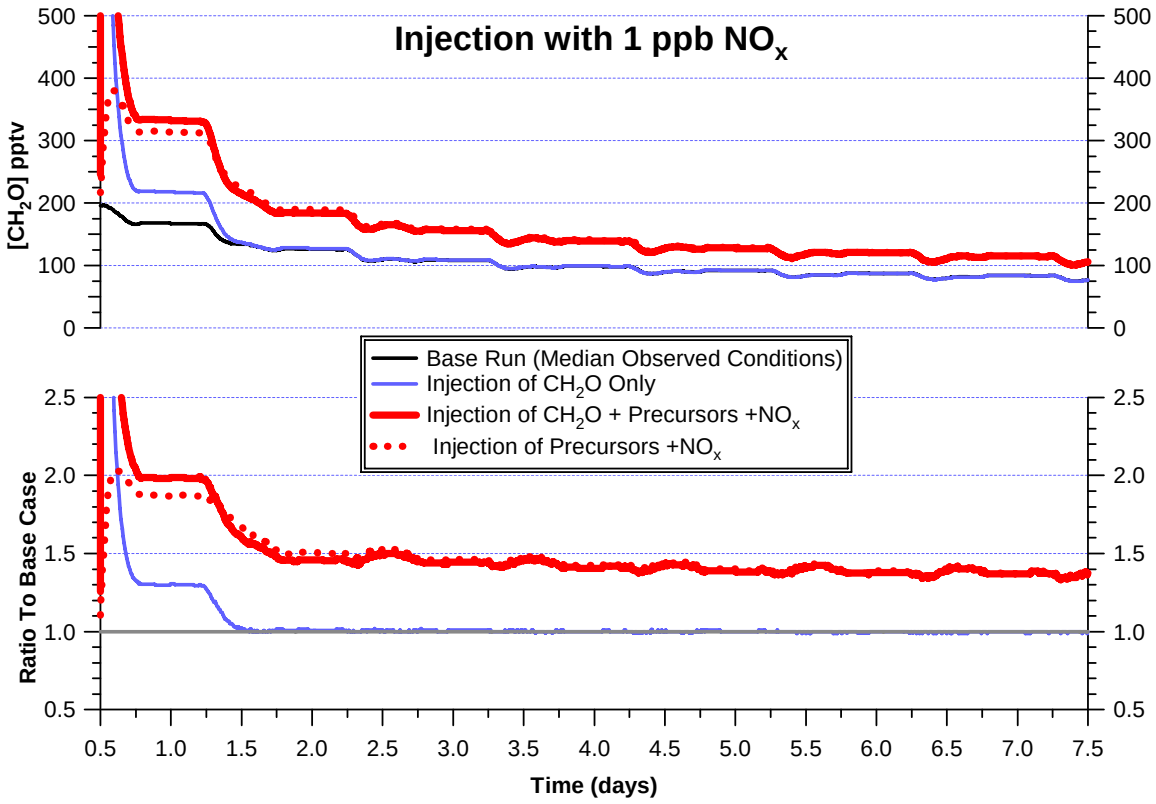

Figure 2

Figure 2: Same as Fig. 1 only employing injection of 1 ppbv of NO_x input to the model at 9-km.

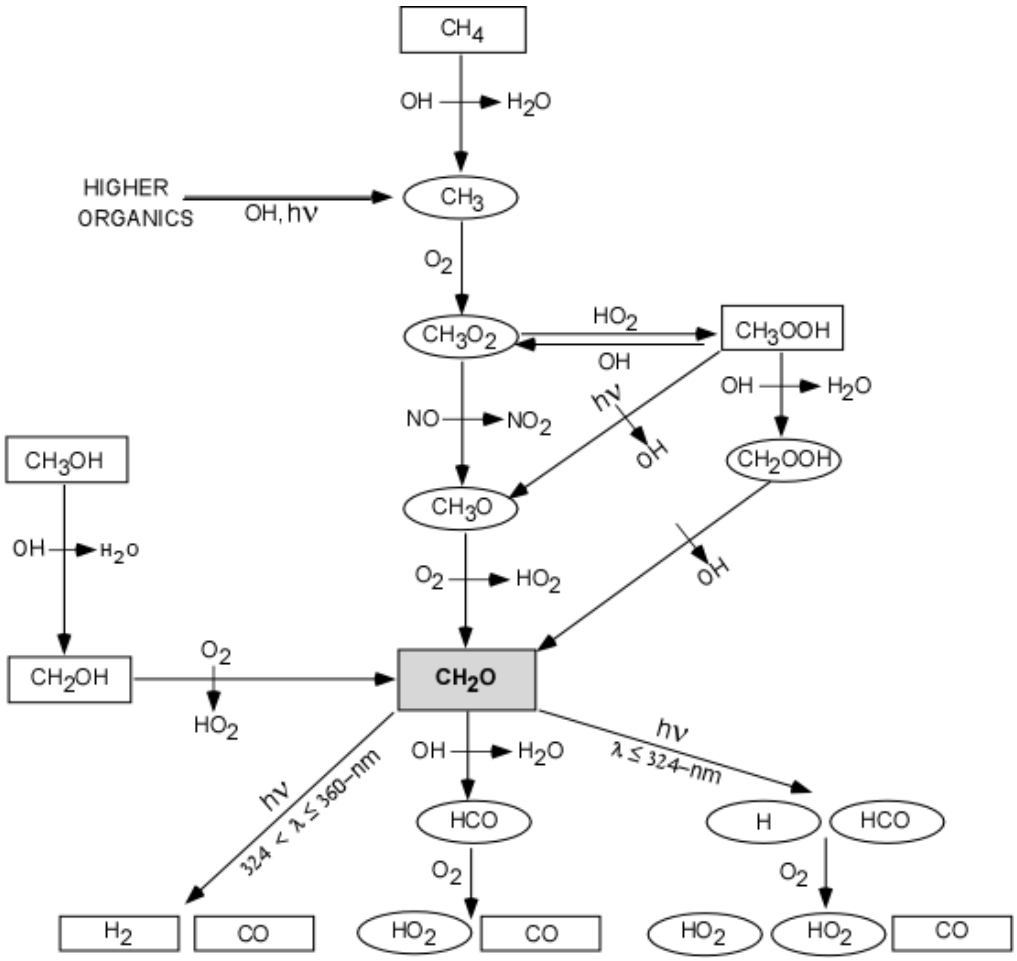

Figure 3: Production and destruction reactions for CH_2O in the troposphere. Destruction from NO_3 and the halogens are not shown nor is the production from organics with Cl. Production of CH_2O from higher organics, which in most cases proceed through the CH_3 radical, are lumped together. Stable species are shown in boxes while reactive transients are shown in circles.

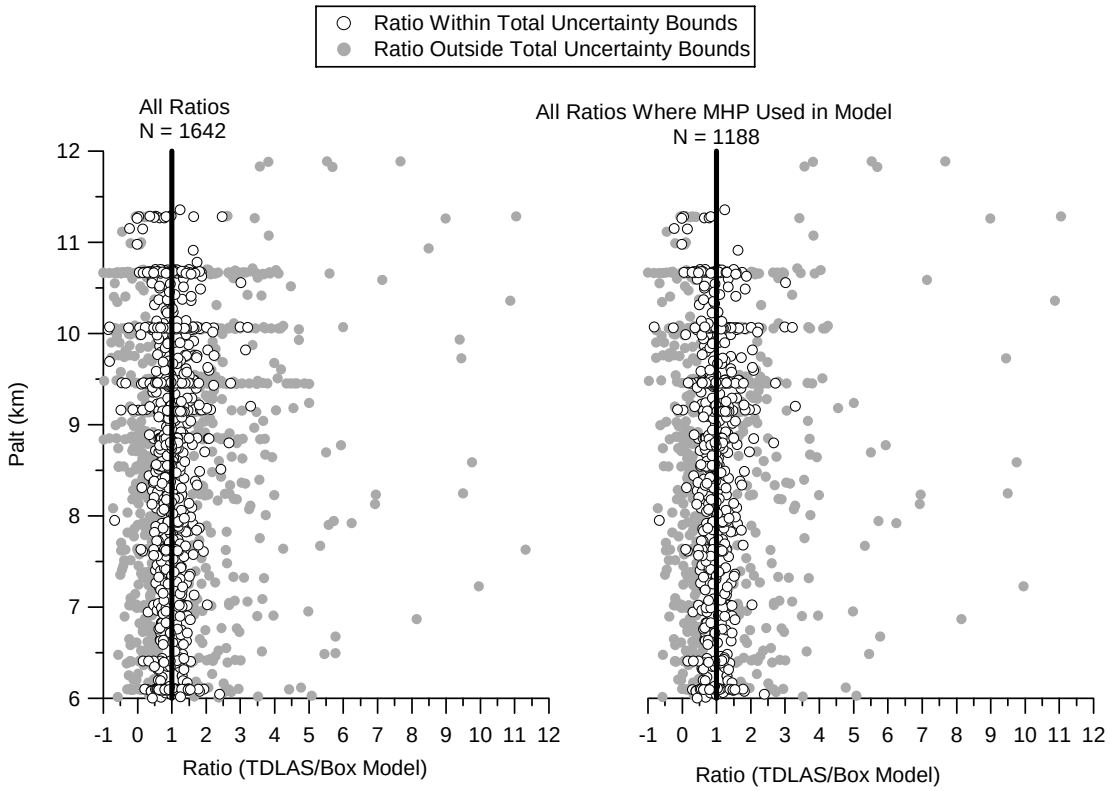

Figure 4

Figure 4: TDLAS/Box Model ratios in the UT for all locations combined with the data parsed into comparisons falling within the combined random measurement-model uncertainties (open points) and those outside this range (filled gray points). All comparisons are shown in the left panel with the exception of 1 point at 11-km (Ratio = 20.8) to maintain resolution. Model values employed measurements of MHP (CH_3OOH) where available and modeled values of MHP where there were no measurements. The right panel shows this comparison where only measurements of MHP were available and used in the model.

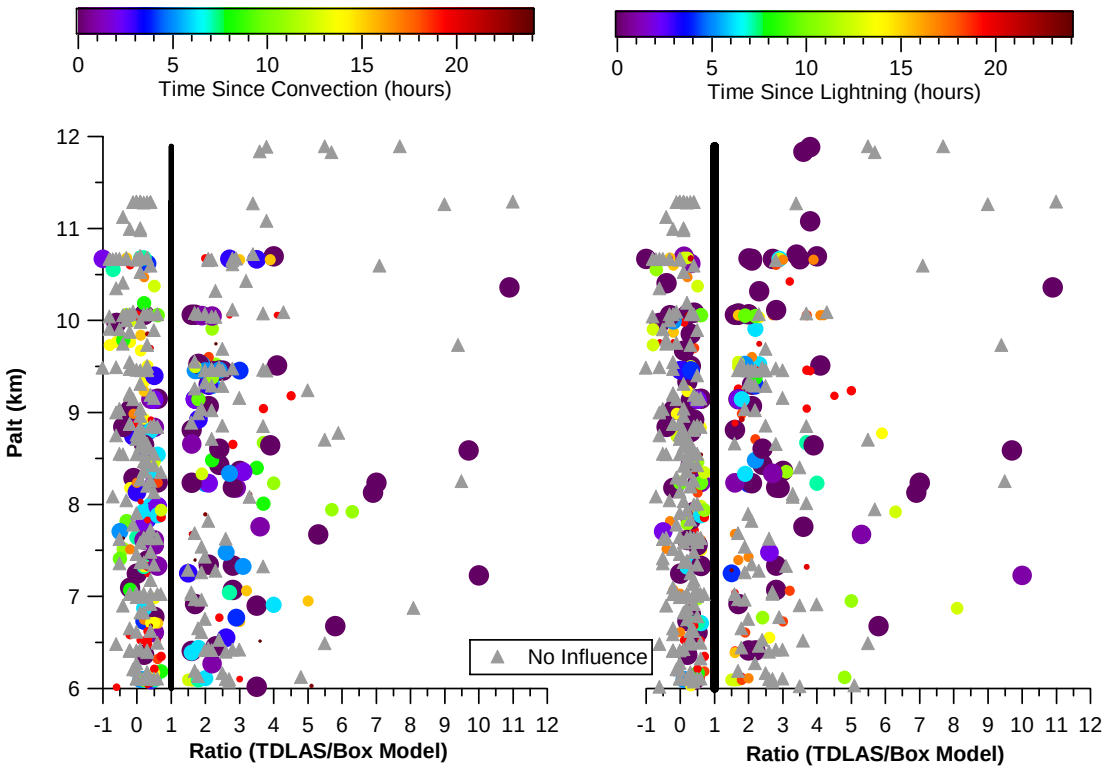

Figure 5

Figure 5: TDLAS/Box Model outlier ratios color coded and sized by the time since convection (left panel) and the time since lightning (right panel). The filled gray triangles are points where there is no convective or lighting influence. The model in all cases is constrained by MHP observations.

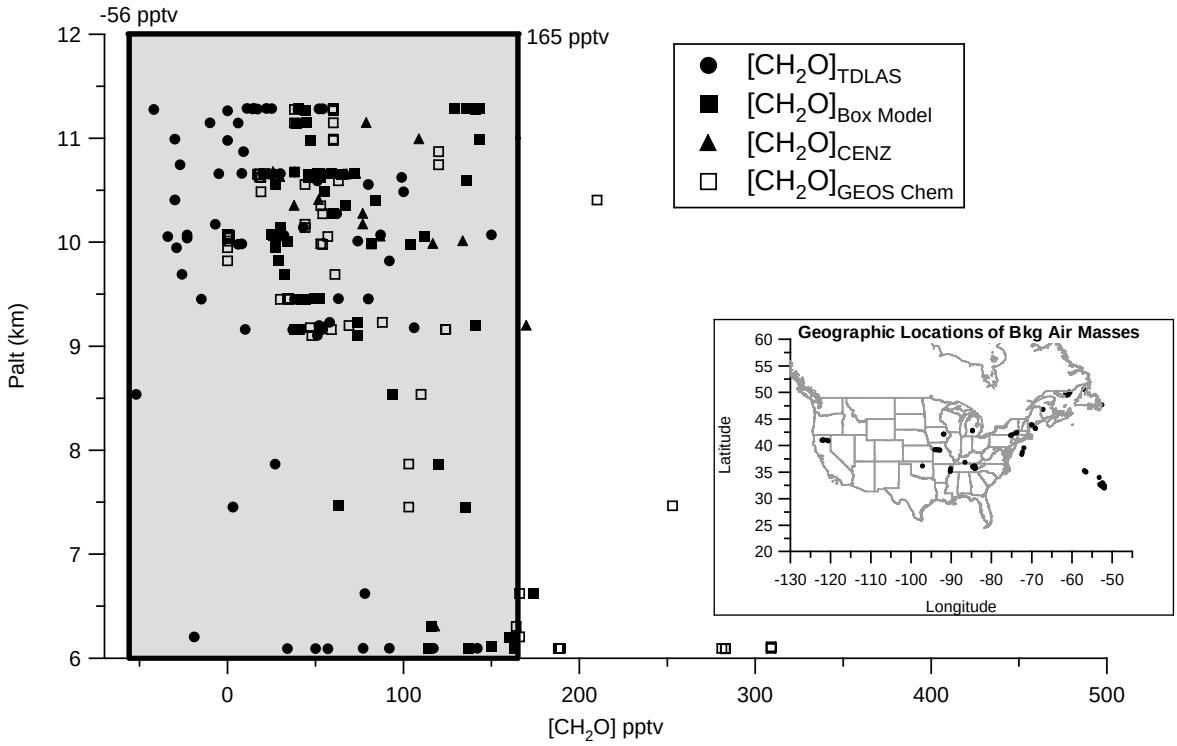

Figure 6

Figure 6: Background UT measurements and model results (N = 68 for TDLAS; N = 62 for Box Model; N = 18 for CENZ; and N = 77 for GEOS-Chem). The limits of -56 pptv to 165-pptv were determined using the various criteria discussed in the text, and the shaded region encompassing these limits captures 99% of the composite measurements and box model results in the UT. The inset depicts the geographic location where these samples were acquired.

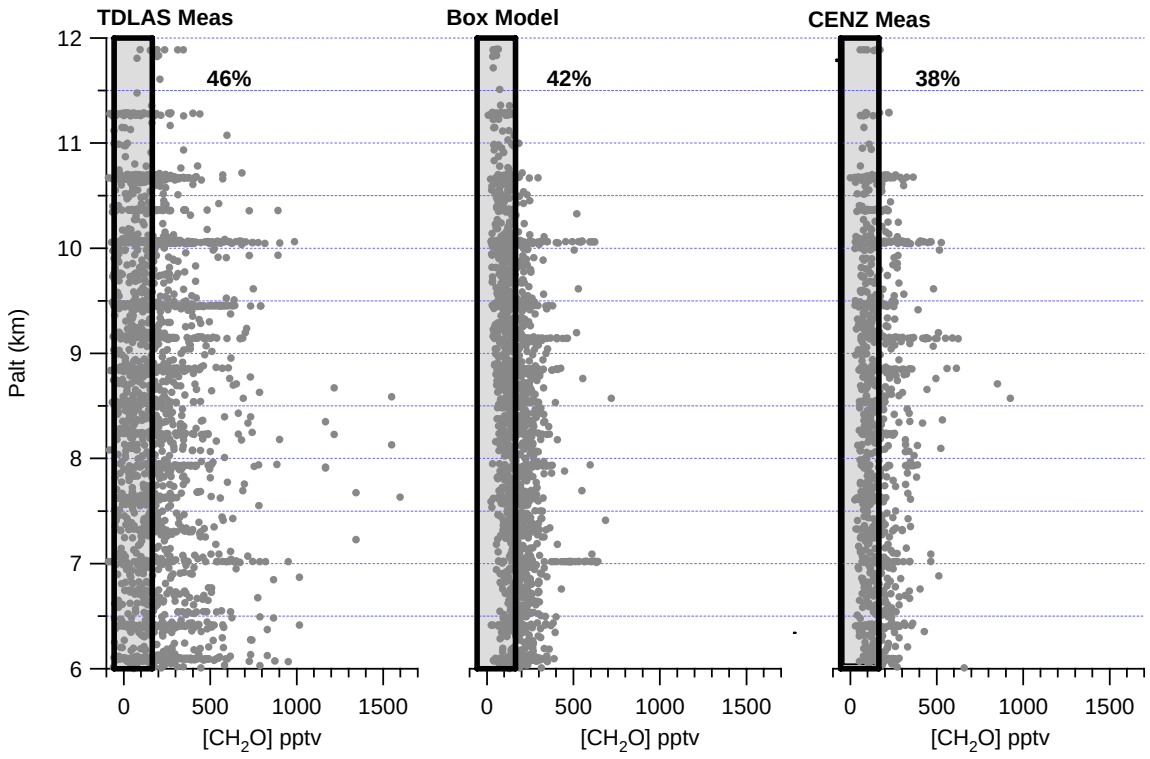

Figure 7

Figure 7: TDLAS, Box model, and CENZ results in the 6-12 km UT range for all data not restricted to location, time coincidence, or MHP measurements available for model input. The (-56 to 165-pptv) background limits defined in the text are indicated on these plots in the shaded regions within the dark rectangles. Indicated with each plot are the percentages of the total UT observations or model results exceeding the 165-pptv background limit.

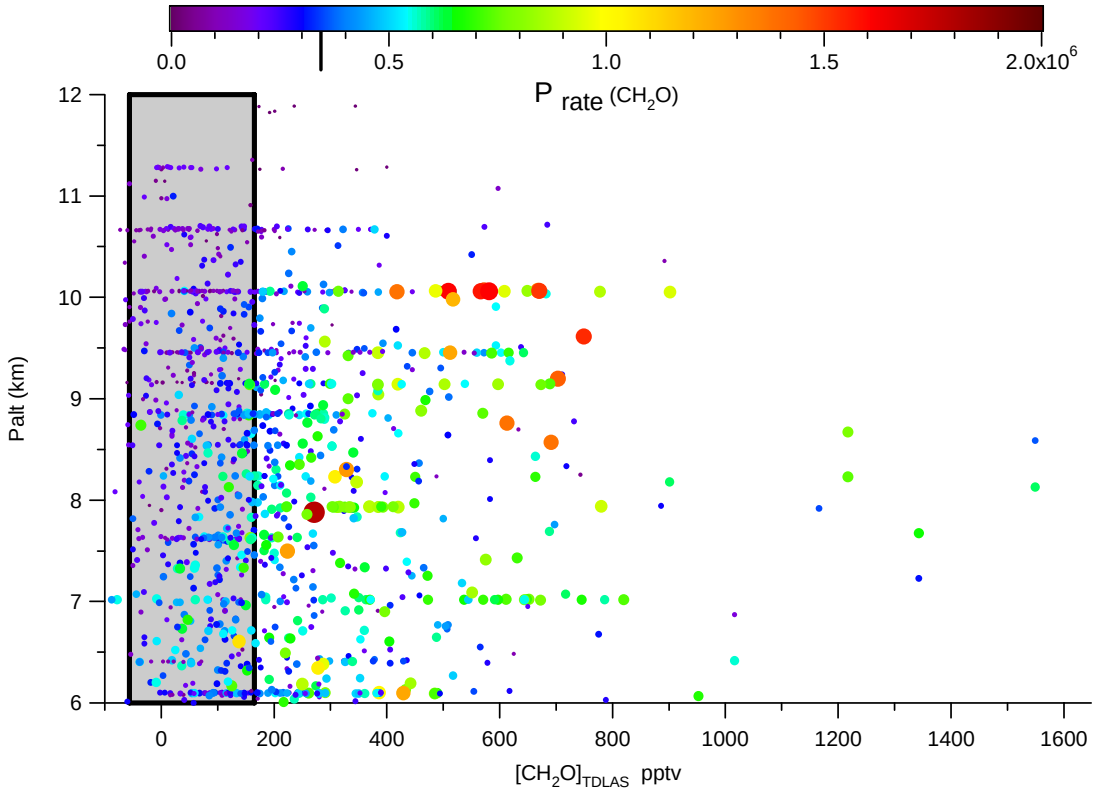

Figure 8

Figure 8: UT TDLAS measurements of CH_2O that are time coincident with the box model calculations (N = 1188) where measurements of MHP are used as model input. Similar to Fig. 7, the background range is shown in the shaded region within the dark rectangle. The points are color coded and sized by the box model CH_2O production rates, the maximum value for which during the strict 77 background selection criteria (designated by the vertical line in the color scale) is 3.51×10^5 molecules cm^{-3} sec^{-1}.

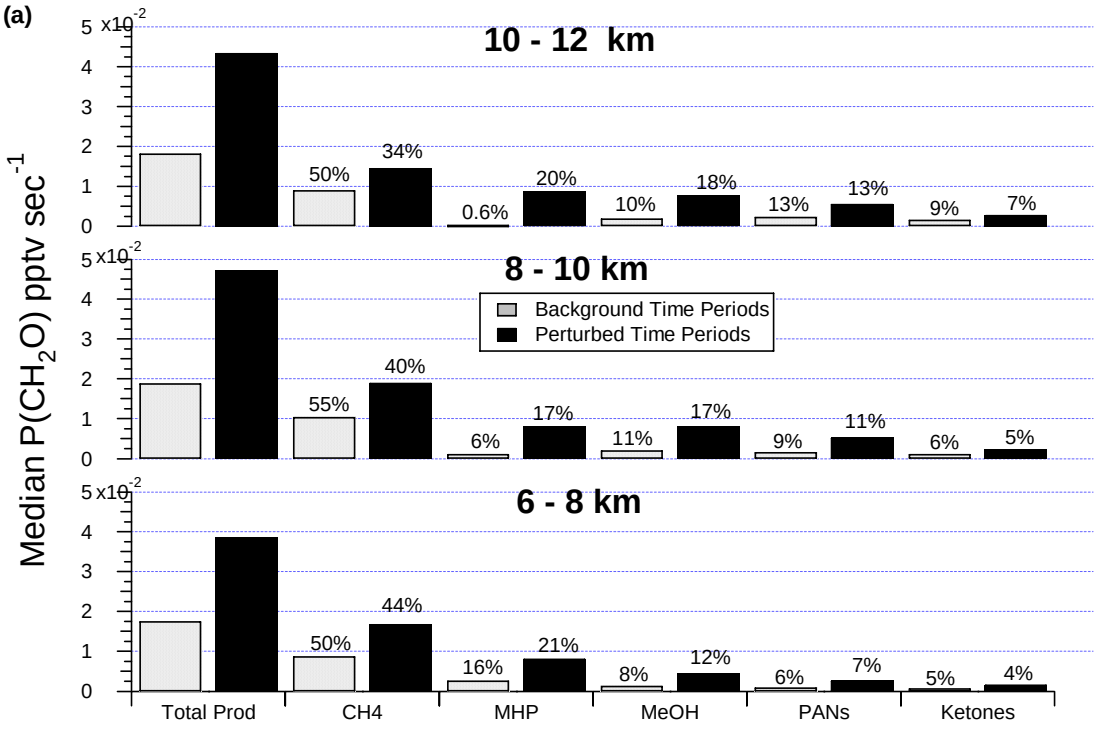

Figure 9

Figure 9a: Median UT CH_2O production rates (in pptv sec^{-1}) for time coincident TDLAS and box model results for background and perturbed time periods when measurements of MHP are used as model constraints. These results are from the box model for the major production terms only, MHP is CH_3OOH, MeOH is methanol, PANs represent production from PAN and RCO_3 type compounds, and Ketones includes acetone and other ketones. The numbers above each term represent the production percentage for that air mass type in the given altitude bin.

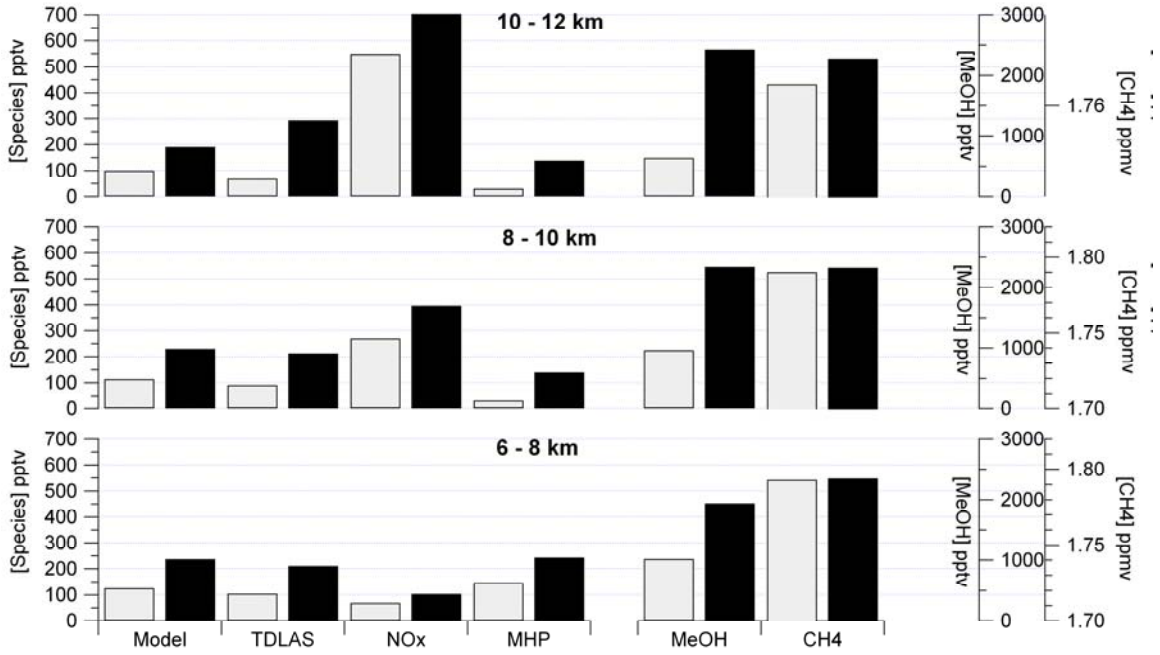

Figure 9b: Corresponding median mixing ratios for CH_2O along with those involved in the 3 major production terms (CH_4, MHP, and Methanol) plus NO_x calculated in the same format as Fig. 9a. The methanol (MeOH) and CH_4 mixing ratios are referenced to the axes on the right while the other species employ the left axis. The NO_x mixing ratio in the 10-12 km perturbed case is off scale (1391 pptv).

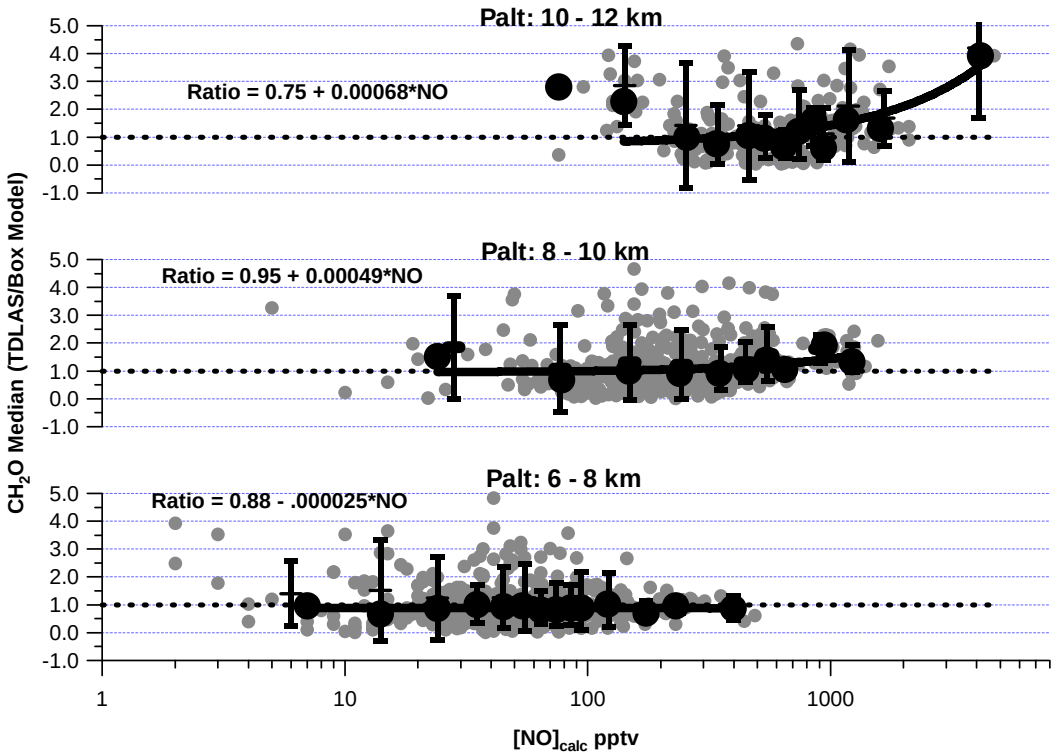

Figure 10

Figure 10: Binned CH_2O measurement (TDLAS/Box Model) ratio as a function of binned NO (from NO_2 measurements and photostationary state calculations) for 3 pressure altitudes in the UT. Calculations were only performed for time coincident TDLAS and box model results where MHP was used in the model constraint. The filled black circles are binned median ratios versus binned median NO, the horizontal lines are the binned averaged ratios versus binned averaged NO with 1 standard deviation limits, and the light gray points are the individual ratios. The solid dark lines are linear fits of the binned median values for each altitude bin, and the results of these fits are shown with each altitude bin. The first binned point in the 10-12 km range was not included in this fit since there were only 3 points in this bin. For resolution these plots are restricted to ratios less than 5.5: in the 10 -12 bin there are 8 points not shown higher than this, in the 8 – 10 and 6 – 8 km ranges there are 7 and 5 points, respectively higher than this. The fits appear curved here when plotting a linear fit on a semi-log axis.

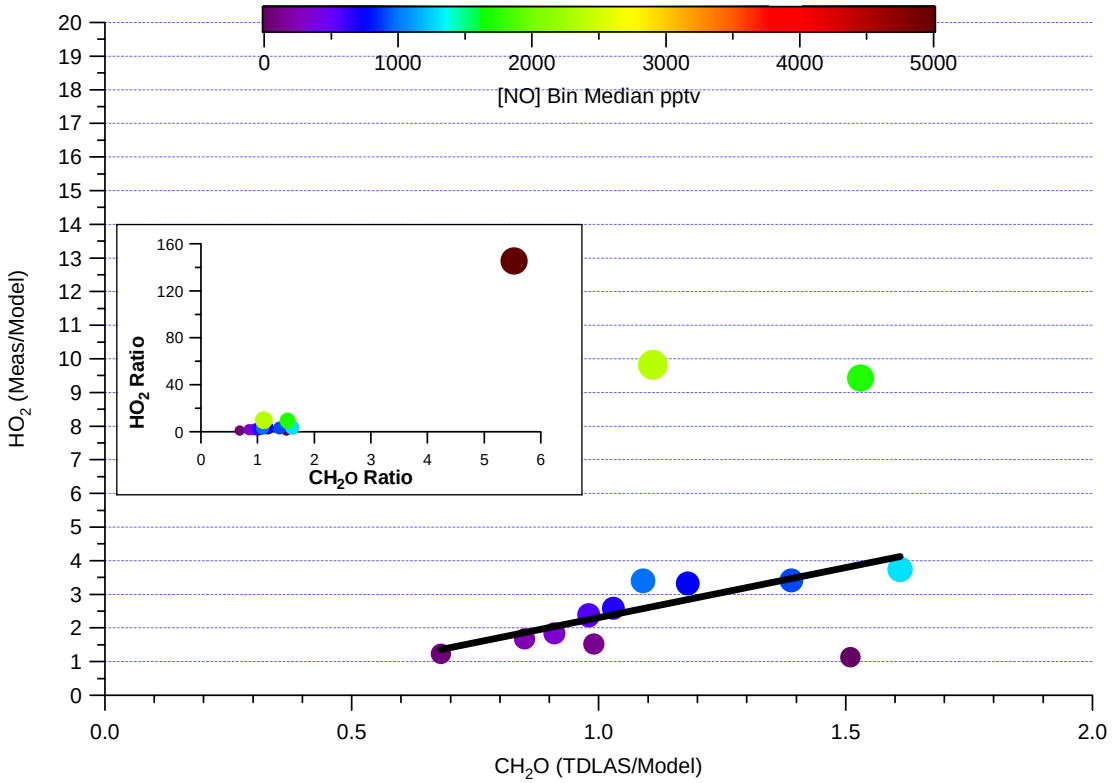

Figure 11

Figure 11: Median HO_2 (measurement/model) versus CH_2O (measurement/model) ratios in the 8 – 12-km altitude range binned by the median value of NO calculated. This plot shows data only when there were CH_2O measurement-model comparison points when the model was constrained by MHP measurements. The data are colored and sized by the binned NO median values. The solid line is a linear fit of the 11 points with NO values < 1500-pptv (slope = 3.0 ± 0.3, r^2 = 0.76). The anomalously low point at a CH_2O ratio of 1.5 was not included in this fit due to sparseness in the data in this bin. The two very high points for median NO values exceeding 1500-pptv give rise to a more rapidly increasing HO_2 discrepancy than CH_2O and were not included in the fit. The inset further shows these two points on an expanded scale along with an additional very large discrepancy in both HO_2 and CH_2O at a binned median NO value of 4748-pptv. These 3 elevated NO points perhaps indicate a regime where HO_x is directly formed without CH_2O.

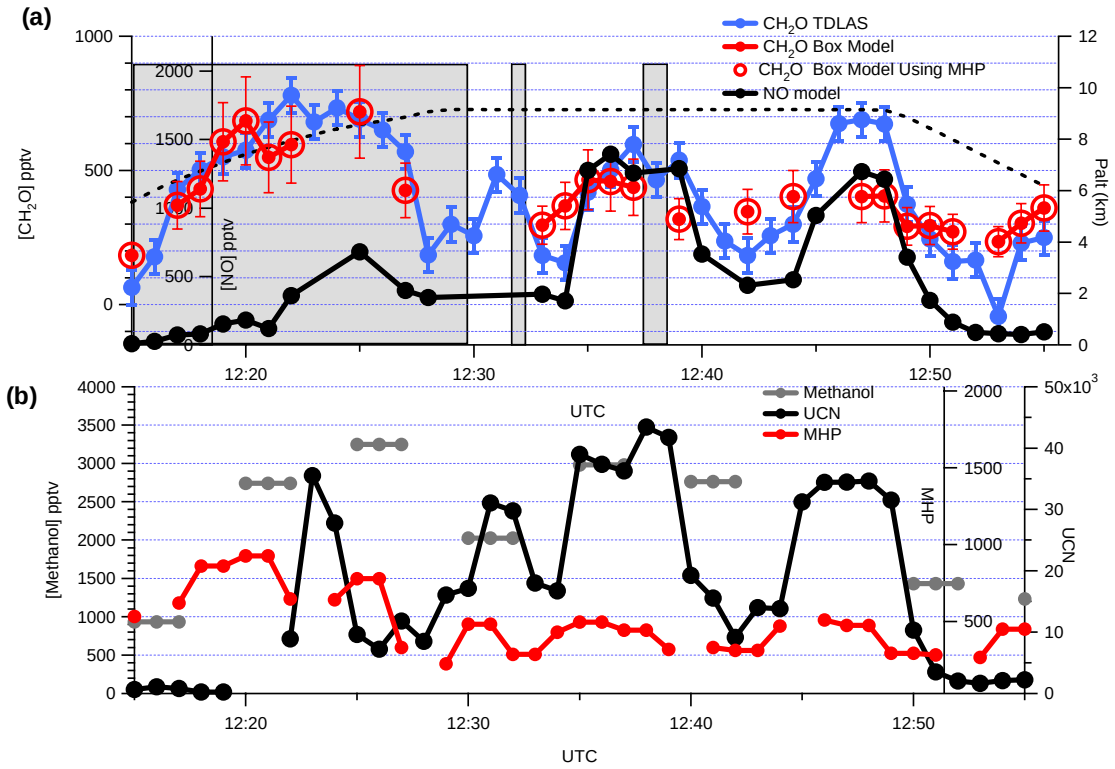

Figure 12

Figure 12a,b: Convective outflow event on August 11, 2004. The shaded regions in **(a)** indicate when the DC-8 was sampling in non-clear regions (clouds, haze, and intermediate haze). At 12:20 and 12:21 the DC-8 was in clouds. The TDLAS and box model error bars are the random uncertainties at the 2σ level and the dashed line in **(a)** indicates the pressure altitude using the right hand axis.

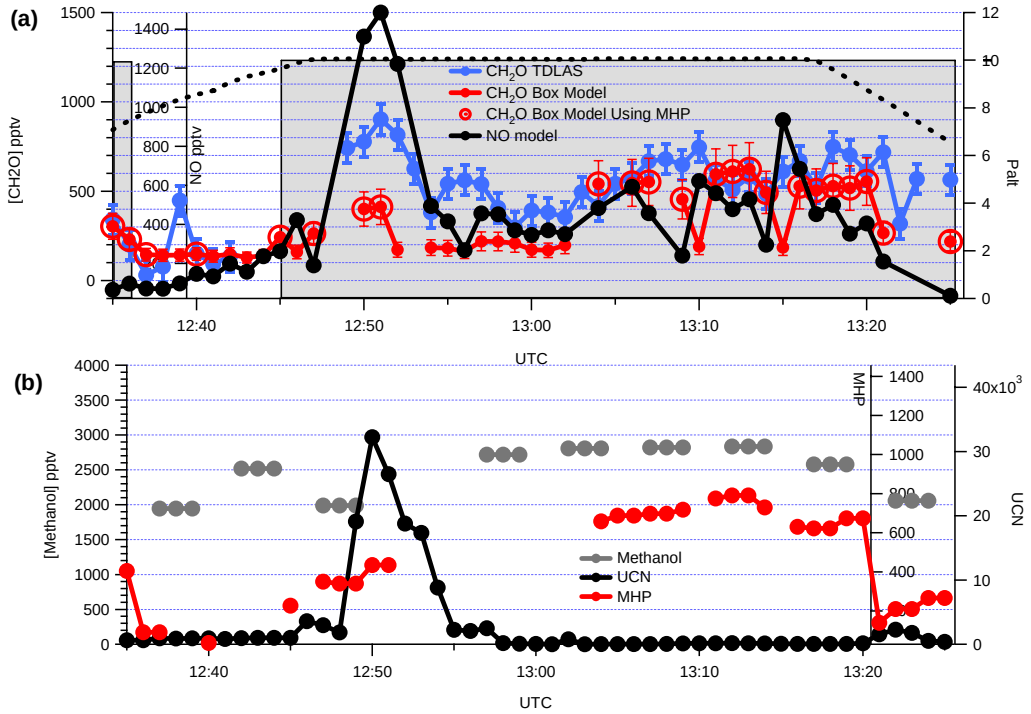

Figure 13

Figure 13: Plots similar to Fig. 12 only for convection during August 6, 2004.

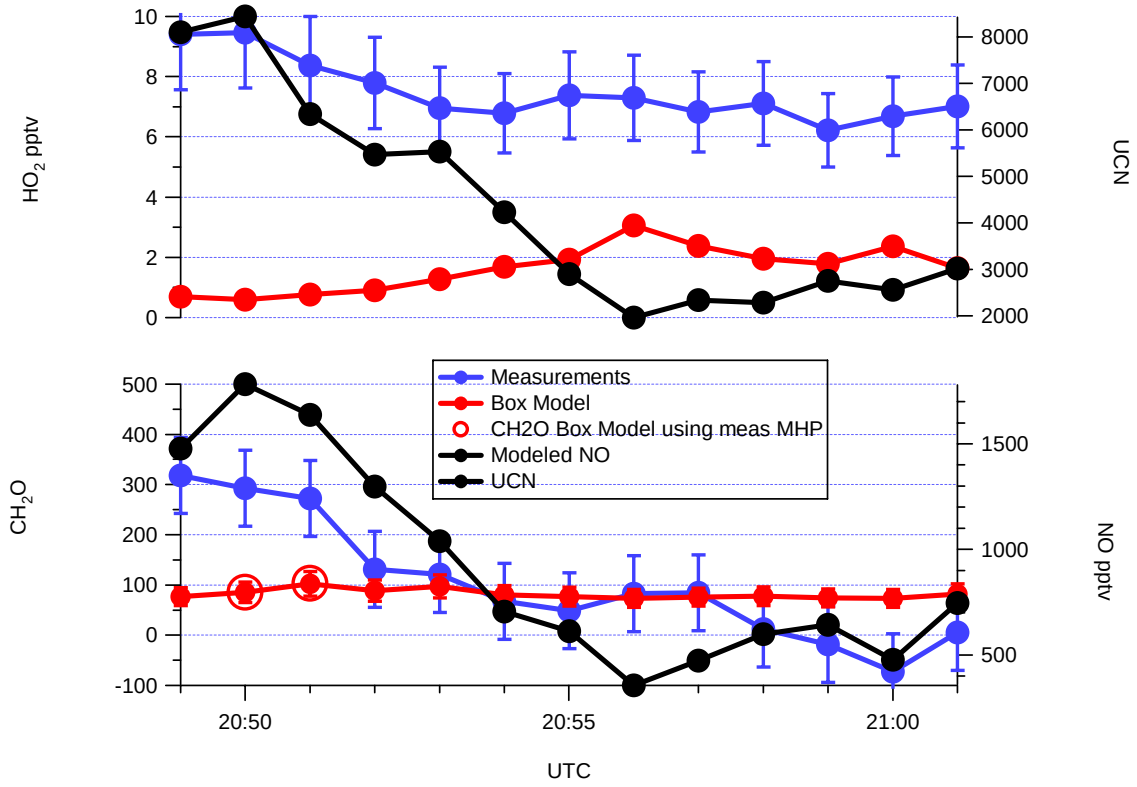

Figure 14

Figure 14: CH_2O and HO_2 measurements and box model values for a flight leg on July 8, 2004 at 10.7-km over South Carolina. The calculated NO mixing ratios and measured UCN (right axes) are also shown.